J. Fluid Mech. (1991), *vol.* 230, *pp.* 1–44
Printed in Great Britain

Low-Reynolds-number turbulent boundary layers

By LINCOLN P. ERM† AND PETER N. JOUBERT
Department of Mechanical Engineering, University of Melbourne, Parkville, Victoria 3052, Australia

(Received 28 February 1990 and in revised form 25 January 1991)

An investigation was undertaken to improve our understanding of low-Reynolds-number turbulent boundary layers flowing over a smooth flat surface in nominally zero pressure gradients. In practice, such flows generally occur in close proximity to a tripping device and, though it was known that the flows are affected by the actual low value of the Reynolds number, it was realized that they may also be affected by the type of tripping device used and variations in free-stream velocity for a given device. Consequently, the experimental programme was devised to investigate systematically the effects of each of these three factors independently. Three different types of device were chosen: a wire, distributed grit and cylindrical pins. Mean-flow, broadband-turbulence and spectral measurements were taken, mostly for values of R_θ varying between about 715 and about 2810. It was found that the mean-flow and broadband-turbulence data showed variations with R_θ, as expected. Spectra were plotted using scaling given by Perry, Henbest & Chong (1986) and were compared with their models which were developed for high-Reynolds-number flows. For the turbulent wall region, spectra showed reasonably good agreement with their model. For the fully turbulent region, spectra did show some appreciable deviations from their model, owing to low-Reynolds-number effects. Mean-flow profiles, broadband-turbulence profiles and spectra were found to be affected very little by the type of device used for $R_\theta \approx 1020$ and above, indicating an absence of dependence on flow history for this R_θ range. These types of measurements were also compared at both $R_\theta \approx 1020$ and $R_\theta \approx 2175$ to see if they were dependent on how R_θ was formed (i.e. the combination of velocity and momentum thickness used to determine R_θ). There were noticeable differences for $R_\theta \approx 1020$, but these differences were only convincing for the pins, and there was a general overall improvement in agreement for $R_\theta \approx 2175$.

1. Introduction

A low-Reynolds-number turbulent boundary layer is said to exist when the Reynolds number based on momentum thickness, R_θ, is less than about 6000. Such flows play an important role in many fluid-flow problems including flow through turbomachinery, flow over wings, numerical modelling and model testing in wind tunnels. Despite the importance of these flows, there still remain many significant unanswered questions regarding their behaviour. In the past the problem of understanding the flows has been attacked on at least three different fronts. Firstly, researchers have taken measurements using pressure probes and/or hot-wire probes. Secondly, flow visualization has been used to look at flow structure and thirdly, flow

† Present address: Aeronautical Research Laboratory, 506 Lorimer Street, Port Melbourne, Victoria, 3207, Australia.

prediction, using models of varying degrees of complexity, has been used. This investigation is concerned with the first of these approaches and is a summary of the work of Erm (1988). In this paper, the presentation of reliable experimental data is of prime importance.

1.1. *Survey of relevant literature*

Coles (1956) carried out an extensive survey of mean-velocity profile measurements at high Reynolds numbers and proposed that the velocity profile outside the viscous sublayer could be accurately described by

$$\frac{U}{U_\tau} = \frac{1}{\kappa}\ln\left(\frac{yU_\tau}{\nu}\right) + C + \frac{\Pi}{\kappa} w\left[\frac{y}{\delta}\right]. \tag{1}$$

U is the mean velocity in the layer in the longitudinal direction at a distance y from the surface and U_τ is the friction velocity, given by $U_\tau = (\tau_w/\rho)^{\frac{1}{2}}$, where τ_w is the wall shear stress and ρ the fluid density. ν denotes the kinematic viscosity and κ and C are the logarithmic-law constants which have values of 0.40 and 5.1 respectively. Π is a profile parameter and for zero-pressure-gradient flows it has a value of approximately 0.55. The function $w[y/\delta]$, where δ is the boundary-layer thickness, is termed the 'law of the wake'. Throughout this paper, square brackets are used to denote a functional dependence. Also, U/U_τ and yU_τ/ν will often be denoted simply by U^+ and y^+ respectively.

Mean-flow behaviour is known to be affected by low Reynolds numbers, but different researchers have given differing opinions on how the flow changes. Areas of controversy have been whether the logarithmic region disappears and whether it has changing values of κ and C, as the Reynolds number is decreased. The wake component of the flow is also known to change at low Reynolds numbers, but the changes have been interpreted in a number of different ways by researchers.

Preston (1958) examined the possible disappearance of the logarithmic region and indicated that for $R_\theta = 389$ the region disappeared. He also indicated that $R_\theta = 320$ was about the minimum Reynolds number for which fully developed turbulent flow could be observed experimentally on a flat plate. Granville (1977) indicated that the region disappeared when $R_\theta = 738$.

Coles (1962) extended his initial work by analysing virtually all of the published data on low-Reynolds-number flows on smooth flat surfaces in nominally zero pressure gradients. He determined U_τ from velocity profiles by fitting the data in the logarithmic region to the line having constants $\kappa = 0.41$ and $C = 5.0$. Coles identified a normal state for the layer at constant pressure and expressed this state in terms of his now well-known relationship between $\Delta U/U_\tau \equiv \Delta U^+$ and R_θ (see figure 2), where ΔU^+ is the maximum deviation of a profile from the logarithmic law. Coles constructed balances of momentum using the determined values of U_τ and found that the balances were acceptable. Thus he confirmed the form of his relationship and indicated that the logarithmic law, with $\kappa = 0.41$ and $C = 5.0$, applied at low Reynolds numbers. He indicated that (1), which was developed for high Reynolds numbers, is still valid provided ΔU^+, or equivalently $2\Pi/\kappa$, varies with R_θ in the way he specified. The asymptotic value of ΔU^+ given by Coles is about 2.7, which corresponds to a value of Π of about 0.55.

Simpson (1970) extended Coles' (1956) high-Reynolds-number work to low Reynolds numbers. He proposed that κ and C vary with R_θ for $1000 < R_\theta < 6000$ and he asserted that the reduction of the wake with decreasing R_θ could be accounted for

by varying κ and C and holding Π constant. This is in complete contrast to Coles (1962) and the contradiction requires some explanation.

Huffman & Bradshaw (1972) investigated this contradiction by analysing low-Reynolds-number duct flows. They chose these flows since they realized that the highly turbulent outer region associated with them would presumably have a greater effect on the inner layer, and thus on the values of κ and C, than would the outer region of boundary-layer flows, which are much less turbulent, so therefore if κ and C were found to be constant for Reynolds number variation for duct flows, then κ and C would also be constant for boundary-layer flows. Their results showed that κ appeared to be a constant to good accuracy and that C was Reynolds-number dependent. However, they indicated that even the variation of C is likely to be small in boundary layers unless the influence of the outer layer is extremely large. The values of the constants corresponding to boundary layers were $\kappa = 0.41$ and $C = 5.0$.

The work of Murlis (1975) and Murlis, Tsai & Bradshaw (1982) represents a very significant contribution to our understanding of low-Reynolds-number flows. Mean-flow and turbulence measurements were taken in a zero pressure gradient for values of R_θ ranging from 791 to 4750. The tripping device used was a 0.03 in. (0.76 mm) wire and the nominal velocity was 50 ft/s (15.2 m/s). Their results strongly suggest that the logarithmic law applies unchanged down to $R_\theta = 700$. For $\kappa = 0.41$ and $C = 5.2$, their ΔU^+ data agreed reasonably well with Coles' (1962) curve. Reynolds stresses and triple products for u and v, but not w, were given, where u, v and w denote the fluctuating components of velocity about the mean in the longitudinal or x, normal or y and transverse or z directions respectively. All of their turbulence measurements were outside the logarithmic region. Although no w measurements were actually taken, $\overline{w^2}$ terms were approximated from the measured $\overline{u^2}$ and $\overline{v^2}$ terms, where overbars denote time-averaged quantities. The researchers did not present any spectra.

Purtell (1978) and Purtell, Klebanoff & Buckley (1981) studied low-Reynolds-number flows in a zero pressure gradient. The profiles presented, both for mean velocities and intensities, were taken with a hot-wire probe. Measurements were taken for values of R_θ varying from 465 to 5200. The velocities ranged from 2.3 to 11.6 m/s and two sandpaper tripping devices were used. Altogether at least six different flows were used for measurements, where the different flows corresponded to different combinations of device and velocity. Often plots were given to show how a quantity varied with R_θ, but the points on these plots corresponded to different flows, thus implying that only the value of R_θ was important and that it was immaterial how R_θ was formed. The values used for the logarithmic-law constants were $\kappa = 0.41$ and $C = 5.0$ and they showed that these values of κ and C did not vary with R_θ. The extent of the logarithmic region was found to decrease with decreasing R_θ but the region did not disappear at low values of R_θ. They also compared their ΔU^+ data with the relationship proposed by Coles (1962) and found that the asymptotic curve differed somewhat from that of Coles in that ΔU^+ did not disappear for low values of R_θ. Intensities in terms of u were presented, but no data in terms of v and w were given. Purtell presented three families of u-spectra.

Smits, Matheson & Joubert (1983) studied low-Reynolds-number flows on a flat plate in both a zero and two favourable pressure gradients for $R_\theta < 3000$. The following discussion will apply to the zero-pressure-gradient results. An extensive range of mean-flow measurements, but no turbulence measurements, were presented. Measurements were taken for at least five different velocities and the layers were generally tripped by using cylindrical pins. For $R_\theta > 1000$, the data agreed

reasonably well with Coles' (1962) Π curve. It was assumed that $\kappa = 0.41$ and $C = 5.2$ and that both of these parameters were unaffected by Reynolds number. Checks confirmed the acceptability of using these values of κ and C. A logarithmic region was found to exist for R_θ as low as 354. They indicated that the variation of Π, C_f and H with R_θ, appeared to be independent of how R_θ was formed. C_f is the local skin-friction coefficient given by $C_f = \tau_w/(0.5\rho U_e^2)$, where U_e is the longitudinal velocity at the edge of the boundary layer; H is the shape factor given by $H = \delta^*/\theta$, where δ^* is the displacement thickness.

1.2. *Scope of current investigation*

The preceding survey broadly outlines our current understanding of mean-flow and turbulence characteristics of low-Reynolds-number flows. In the light of this survey, an experimental programme comprising mean-flow and turbulence measurements was developed. The aim was to concentrate on critical areas of concern and to attempt to clarify some of the outstanding questions.

When developing the programme, a question that had to be answered was what type of tripping device to use. The above survey indicates that different researchers have used different types of device to trip their layers, which tends to suggest that they have thought that the type of device used is not all that important. This assumption is consistent with the fact that Coles' (1962) ΔU^+ curve was based on data from nine investigations in which different devices were used. However, the fact remains that even though this curve may not be significantly affected by the device used, other mean-flow and turbulence characteristics may depend upon the device. In the past, researchers have not systematically compared the effects of different devices on low-Reynolds-number mean-flow or turbulence behaviour, so the extent to which flows depend on the device used is unknown. To investigate effects of device, three different types, representative of those used by others, were chosen. These were a circular wire, distributed grit and cylindrical pins. Further details of these will be given in §3.

The general consensus of most researchers after Coles (1962) is that his criterion for a normal state for a low-Reynolds-number flow at constant pressure is basically correct. Thus the flows were established so that they also followed his curve. It is shown in §3 that for these flows, the turbulent energy imparted by the device is just sufficient to cause the turbulent boundary layer to advance to almost the upstream limit of turbulent flow. Such flows are regarded to be correctly stimulated and the corresponding velocity will often be referred to as the design velocity. Further increases in turbulent energy, corresponding to increases in velocity, fail to advance the turbulent boundary layer significantly upstream. To meet the requirement of correct stimulation, it was necessary that the sizes of the devices were selected with considerable care. An empirical technique was devised to determine the heights of the devices to match a velocity so that the resultant flows followed Coles' curve.

The existence of a logarithmic region at low Reynolds numbers with $\kappa = 0.41$ and $C = 5.0$ or 5.2 has by now been well established, so there was no need to investigate this matter any further except to decide which value of C to use. Whenever the current data were compared with the work of Coles (1962), then the values of the constants associated with the data were the same as his, $\kappa = 0.41$ and $C = 5.0$, since it would not have been strictly correct to use other values. In other cases, values of U_τ used to non-dimensionalize plotted data were determined by means of a Clauser chart using $\kappa = 0.41$ and $C = 5.2$, as recommended by Brederode & Bradshaw (1974).

In the literature, very few transverse C_f measurements for low-Reynolds-number

flows have been reported. Such measurements are of importance since they give an indication of the three-dimensionality of a flow and how long a flow takes to settle down after being tripped. A comprehensive range of transverse C_f measurements are presented.

Relatively few low-Reynolds-number broadband-turbulence measurements have been published and it is significant that none of the investigations surveyed present any such measurements for w. Accordingly, broadband-turbulence terms up to quadruple products were measured for u, v and w.

There has not been any thorough investigation of spectra at low Reynolds numbers. Despite this, spectra are very important since they give an insight into the physics of turbulence for such flows and indicate how turbulent energy is distributed over different frequencies. Consequently, spectra for u, v and w were taken.

When a velocity is changed from its design value, the resulting ΔU^+ relationship is known to depart from the ideal form suggested by Coles (1962). However, the degree to which this relationship changes and also how other mean-flow and turbulence characteristics for a given R_θ change with changes in flow velocity for different devices has not been systematically investigated in the past. Researchers have often presented measurements corresponding to a given device, but different free-stream velocities, and the assumption has been that it is only the value of R_θ that is important and not how R_θ was formed. A limited range of measurements were taken to study flow behaviour for operation both below and above the design velocity using the three devices.

2. Experimental apparatus and techniques

The wind tunnel used was an open-return suction type of conventional design. The working section had cross-sectional dimensions of 613×309 mm at the inlet and was 2.5 m long. It had three fixed walls and an adjustable straight wall which was used to set a nominal zero pressure gradient. The smooth flat vertical surface upon which measurements were taken formed one of the walls of the working section and was opposite the adjustable wall. The free-stream turbulence intensity in the working section was about 0.32% for a free-stream velocity of about 9.5 m/s. An intensity of this level is close to the midpoint of the 'moderate' range as classified by Coles (1962). Further details of the tunnel are given by Erm (1988).

The tripping devices were glued onto accurately machined metal inserts that could be bolted into a recess in the smooth wall so that the outer surface of an insert was flush with the smooth wall to high accuracy. The inserts and devices extended right across the smooth wall. The centrelines of the wire and pins and the upstream extremity of the grit were located 80 mm downstream of the contraction outlet. This was the origin for all x-distances. The use of the inserts meant that not only could the devices be changed quickly, but also that a device was exactly the same as previously each time its insert was repositioned. These capabilities were invaluable since it was continually necessary to change from one device to another throughout the course of the experiments.

To obtain consistent sets of measurements throughout the course of the investigation, reference conditions were set so that they corresponded to a given reference Reynolds number per metre, but to simplify presentation in this paper, reference conditions will simply be referred to in terms of the corresponding nominal reference velocity. Pressure differences were measured using a Baratron electronic manometer having a full-scale reading of 1.0 mmHg.

Velocity profiles were taken with a specially made Pitot-static probe which had a round head of diameter 0.72 mm for the measurement of total pressures and another arm for the measurement of static pressures. The probe passed through holes drilled through the smooth wall and was connected to a manual traversing mechanism. The y-values of the experimental points on the velocity profiles were corrected to allow for the proximity of the wall by using the correction proposed by Macmillan (1956). The location where the velocity attained 99.5% of its asymptotic value was used to denote the outer edge of the boundary layer and this thickness is denoted simply by δ.

Constant-temperature hot-wire anemometers of Melbourne-University design, as described by Perry (1982), were used for all of the turbulence measurements. A DISA 55PO5 probe was used for the single-wire measurements. A DISA 55P51 probe was used for the crossed-wire measurements, and this was mounted so that it could be rotated through 90° thus enabling measurements to be taken in both the uv- and uw-planes. For both probes, the DISA tungsten filaments were replaced by Wollaston-wire filaments which were etched to expose a platinum sensor of 5 μm diameter. For all single-wire measurements, the etched length was 0.9 mm, except for three families of spectra where it was 0.8 mm. For all crossed-wire measurements, the etched length of both filaments was 0.8 mm. For the crossed-wire probe, the sensors were nominally $\pm 45°$ to the streamwise direction and the separation of the sensors was 1.0 mm.

The distances of the hot wires from the wall were measured with a microscope using the method outlined by Witt, Watmuff & Joubert (1983).

Both the single- and crossed-wire probes were calibrated by using the dynamic calibration technique developed at the University of Melbourne by Perry and his co-workers. The technique has been documented in detail by Perry (1982) and need not be given here. To take a broadband-turbulence profile, the hot-wire voltage signals were low-pass filtered at 10 kHz and sampled by a PDP 11/10 digital computer using a 12 bit analogue-to-digital convertor and the sampled voltages were stored on magnetic tape for subsequent processing. Sampling was in bursts of 8000 samples and the sampling frequency was 200 Hz. The number of bursts taken at each point was selected to ensure that the cumulative averages of the resulting turbulence terms converged to acceptable limits after the profile had been processed. Near the wall, this limit was typically up to 1% for Reynolds stresses and typically up to 5% for triple products. For points close to the wall it was necessary to sample six bursts, but this was progressively reduced to four or sometimes three bursts by the time the free stream had been reached. The u-broadband-turbulence profiles presented in this paper were taken with the single-wire probe.

All spectra within each family were spaced at fixed values of y/δ. The complete range of values of y/δ used were 0.015, 0.02, 0.03, 0.04, 0.06, 0.08, 0.10, 0.15, 0.20, 0.25, 0.35, 0.45, 0.55, 0.70 and 0.85. Since the boundary-layer thickness was variable and also since there was a limit to how close the hot-wire probes could be taken to the wall, the lower values of y/δ were not obtainable for most families.

The u-spectra were measured with an uncalibrated single-wire probe and the v- and w-spectra with a dynamically matched but uncalibrated crossed-wire probe. The power spectral density of a hot-wire signal was calculated digitally using a fast-Fourier-transform algorithm. The signal was sampled at three different sampling rates to improve the frequency bandwidth of the spectrum at low frequencies and was low-pass filtered at half the digital sampling rate to avoid aliasing of the measured spectrum. The three resulting spectral files were matched and joined to

form a single spectral file and the final spectrum covered a frequency range of 0.1 Hz to 10 kHz. To transform the spectral argument from frequency, f, to streamwise wavenumber, k_1, Taylor's (1938) hypothesis of frozen turbulence was used, i.e. $k_1 = 2\pi f/U_c$, where U_c is the local convection velocity, which was assumed to be equal to the local mean velocity at that point in the flow. In fact there is a spread in convection velocities at a given wavenumber and the implications of this will be discussed in §6, where the spectra are discussed.

The u-spectra were smoothed and normalized such that

$$\int_0^\infty \Phi_{11}[k_1]\,\mathrm{d}k_1 = \overline{u_1^2}, \tag{2}$$

where Φ_{11} is the power spectral density per unit streamwise wavenumber for velocity fluctuations u. Similar expressions in terms of k_1 apply for v- and w-fluctuations.

The technique described above for measuring and reducing spectra is virtually identical to that used by Perry, Lim & Henbest (1987), the only difference being that for the current investigation, the method of smoothing the spectra was slightly different.

3. The establishment of acceptable low-Reynolds-number turbulent boundary layers in a zero pressure gradient

In this section, a technique is proposed for obtaining correctly stimulated low-Reynolds-number flows that show good agreement with Coles' (1962) curve of ΔU^+ *vs.* R_θ.

Three different types of tripping device, namely (*a*) a circular wire, (*b*) distributed silicon carbide grit and (*c*) cylindrical pins, were selected. Although the types of device to be used were chosen at the outset, their heights were unspecified and it was necessary to determine these so that the layers were correctly stimulated at a nominal design reference velocity, which was chosen to be 10.0 m/s. It has been indicated by Erm (1988) that published formulae for determining the heights necessary to cause transition to turbulence can only be used as a guide. One of the reasons for this is that many formulae apply to a device fixed to a flat plate located in the free stream, and not to a device fixed to the tunnel wall, as in the current experiments, where there is a long development of the layer upstream of the device. To overcome this problem, an empirical technique was devised for determining the velocity corresponding to correct stimulation for a device of a given height. Although this approach does not directly satisfy the requirement of determining the device height necessary to produce correct stimulation at 10.0 m/s, it is possible to use the technique and determine the height iteratively. This point will be dealt with in more detail after the technique has been explained.

It was seen to be logical that for a given device there must be some particular velocity at which the device produces correctly stimulated flow. Also, the effectiveness of a given device in tripping a flow could be gauged to some extent by an examination of a plot of the associated C_f *vs.* x relationship. Thus it was reasoned that if a given device was subjected to a series of velocities covering the range of say 8.0 to 14.0 m/s, and plots of C_f made for each velocity within the range, then an examination of the entire family of plots may indicate a velocity that will later, after further testing, be shown to be the velocity that leads to Coles' (1962) relationship being satisfied by the flow. This line of reasoning was validated by actual measurements.

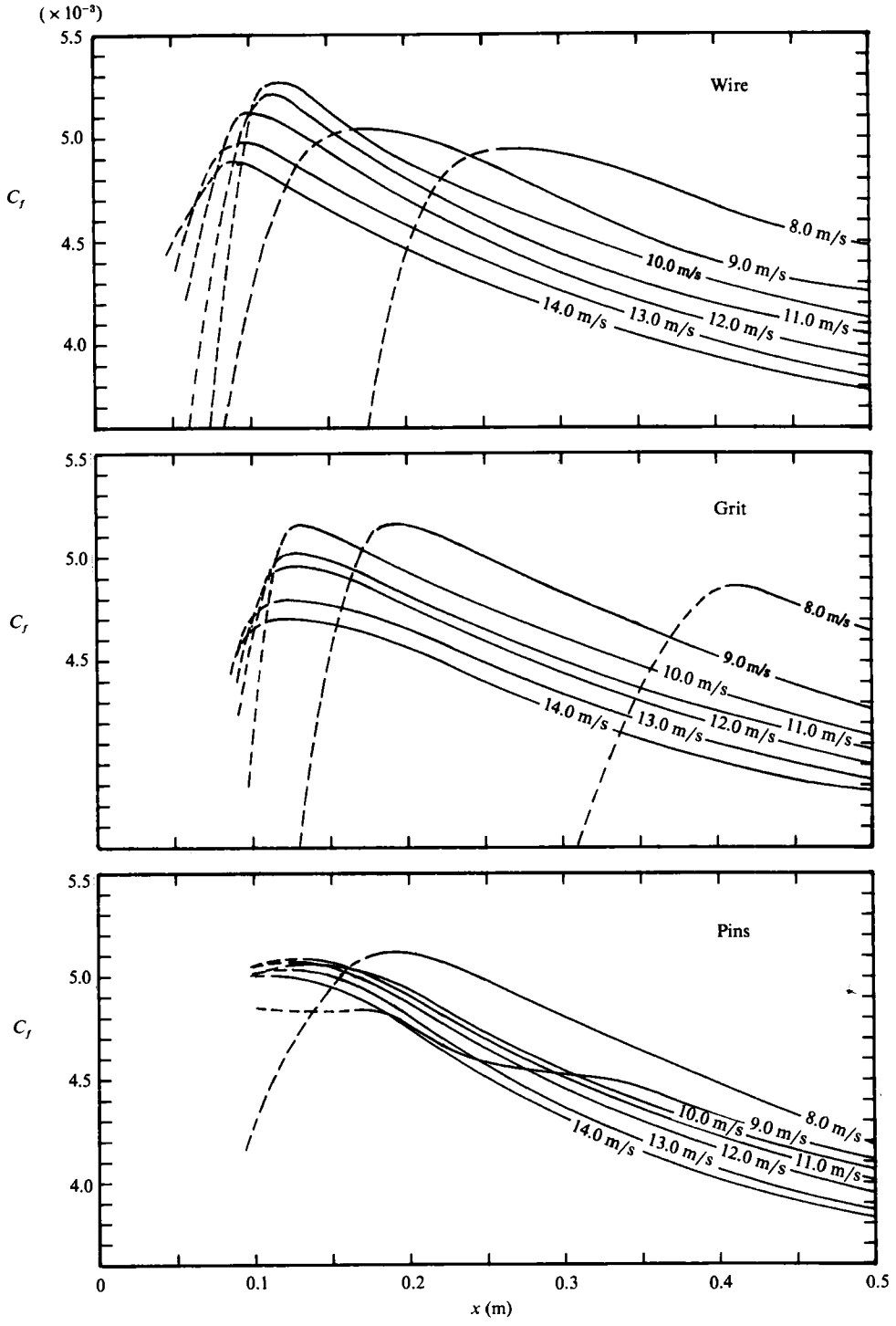

FIGURE 1. Families of centreline values of C_f versus x for three tripping devices and for nominal reference velocities varying from 8.0 to 14.0 m/s.

Figure 1 depicts three families of smoothed curves of C_f for different nominal reference velocities for the three devices and in each case turbulent flow commences just downstream of the peaks of the curves. The parts of the curves that are broken correspond to regions of transition from laminar to turbulent flow. The values of C_f represented by these broken parts are not true values since, along with the rest of the data, they were computed by applying Patel's (1965) calibration to Preston-tube measurements and of course this calibration does not apply in transition regions. When interpreting these curves to select the velocity corresponding to correct stimulation, some latitude is allowed for the case of the pins. The curves for the pins display some unusual behaviour and it is shown in §4.5 that this behaviour is almost certainly related to the transverse distribution of C_f. As the velocity is increased from 8.0 m/s, the devices impart an increased amount of turbulent energy into the flows so that the laminar-to-turbulent transition regions move upstream. It is conjectured that correct stimulation is associated with a particular curve when the peaks of successive curves, corresponding to higher velocities, do not advance significantly upstream. Since the velocity corresponding to the particular curve establishes a turbulent boundary layer almost to the possible upstream limit of turbulent flow, it seems reasonable to assume that the main effect of higher velocities will be to overstimulate the flow. Velocities lower than that corresponding to the particular curve are obviously associated with understimulated flows since the peaks of the curves are well downstream of the device and thus the device is therefore not completely effective in tripping the flow. It is apparent from figure 1 that, for all three devices, the above condition for correct stimulation is satisfied when the velocity is 10.0 m/s. It is a matter of interest that the peaks of the C_f curves for this velocity for the three devices correspond to the highest, or almost the highest, values of C_f indicated by the families of curves for the three cases. The heights of devices necessary to achieve correct stimulation were arrived at iteratively as explained in the following.

When using the above technique, velocity was a dependent variable and could not be prespecified. Consequently, it was generally necessary to try several different heights before finally arriving at the height corresponding to correct stimulation at 10.0 m/s, and some effort was involved in achieving this. It was felt worthwhile to do this for all three devices, however, since this meant that they all would be subjected to the same incident flow and consequently it would be possible to obtain a more meaningful comparison between their stimulating abilities. If all three types of device had been matched with different velocities, then unnecessary complications would have been introduced.

If future researchers wanted to use this method, then it would not in general be necessary for them to go to all this effort since probably they would only use one device and they could judiciously choose its height and settle for the resultant velocity that gives correctly stimulated flow, whose precise value would probably not be all that important.

The heights of the devices determined by the technique for correct stimulation at a velocity of 10.0 m/s are given in table 1, where the important details of the devices are summarized.

Before the above technique is verified, the velocities used to assess the effects of under and overstimulation will first be chosen. The choice was based on the C_f distributions shown in figure 1. When making the choice it was necessary that two conditions were simultaneously satisfied for all devices. Firstly the C_f curves corresponding to the under and overstimulation velocities had to have acceptable

Wire:	Diameter = 1.2 mm
Grit:	Height ≈ 1.6 mm (distance from smooth surface to outermost peaks) Streamwise extent = 50 mm
Pins:	Height = 2.0 mm, diameter = 3.0 mm, spacing = 9.0 mm Pins are of circular cylindrical form

TABLE 1. Details of tripping devices

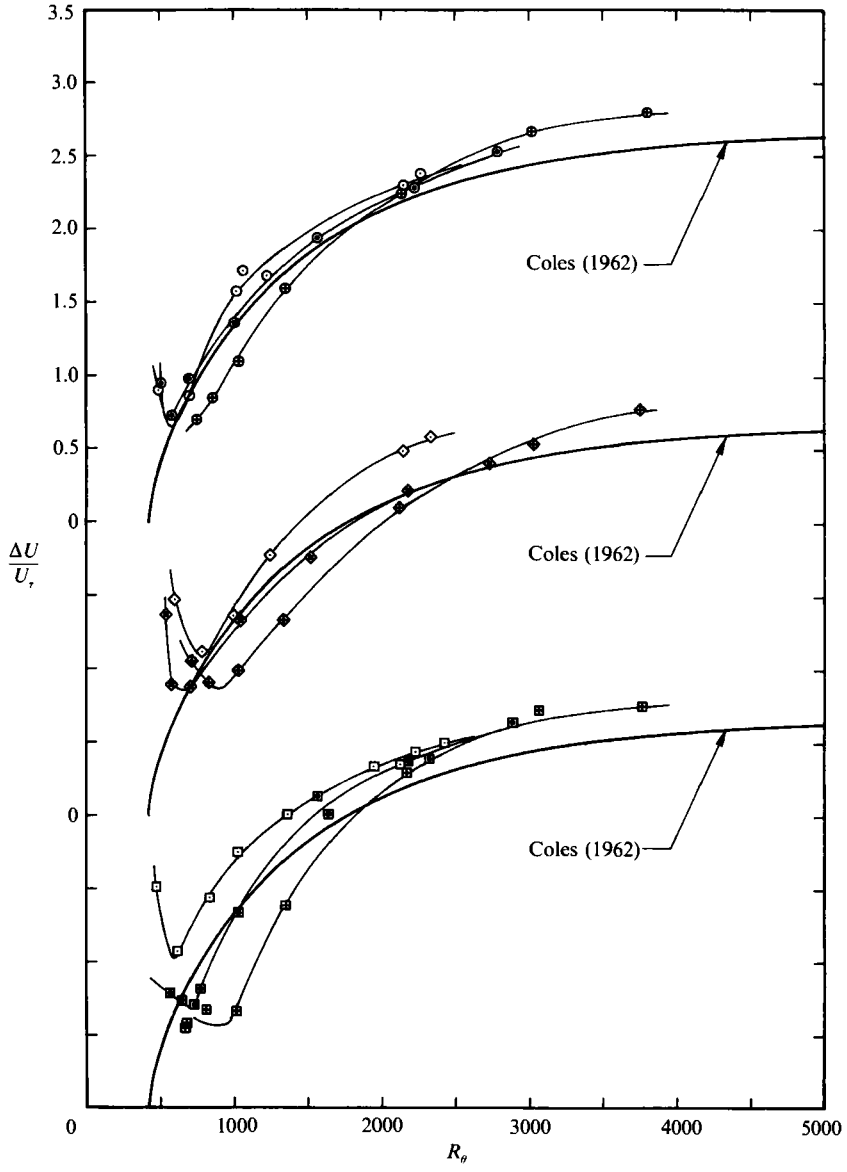

FIGURE 2. Variation of ΔU^+ with R_θ. Note shift in ordinate. Velocities given below are nominal values. Wire: ⊙, 8.0 m/s; ⊙, 10.0; ⊕, 14.0. Grit: ◇, 8.0 m/s; ◈, 10.0; ⊕, 14.0. Pins: ⊡, 8.0 m/s; ▣, 10.0; ⊞, 14.0.

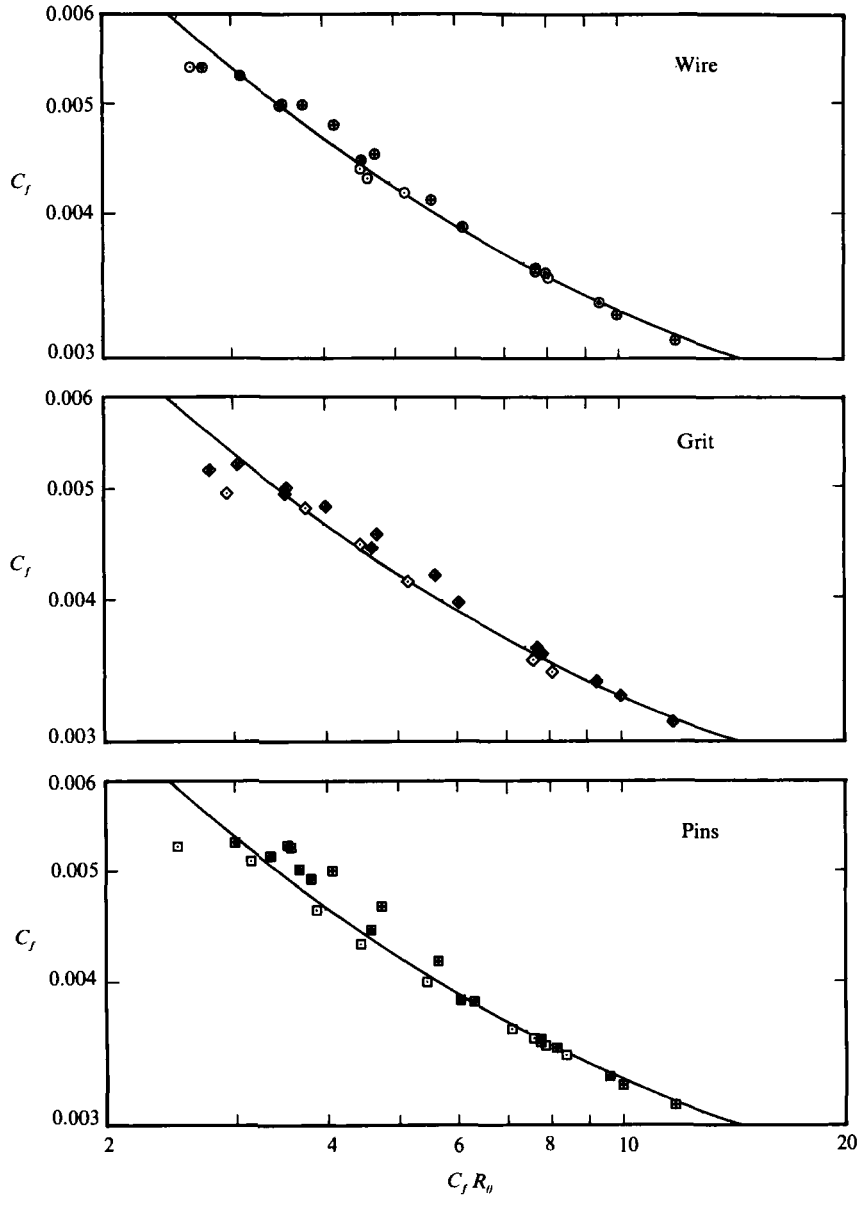

FIGURE 3. Log C_f versus log $C_f R_\theta$. ——, Coles' (1962) curve. For explanation of symbols see figure 2.

shapes and secondly the locations of the maximum values of C_f on these curves, and thus the locations of the commencement of the fully turbulent layers, had to be within acceptable distances from the devices.

A velocity of 8.0 m/s was seen to satisfy both conditions for all devices, although the agreement with the second condition for the wire and grit was only tolerably acceptable, and consequently this velocity was chosen for the understimulated flows. Any velocity above 10.0 m/s could have been chosen for the overstimulated flows since both conditions were always simultaneously satisfied for all three devices. A

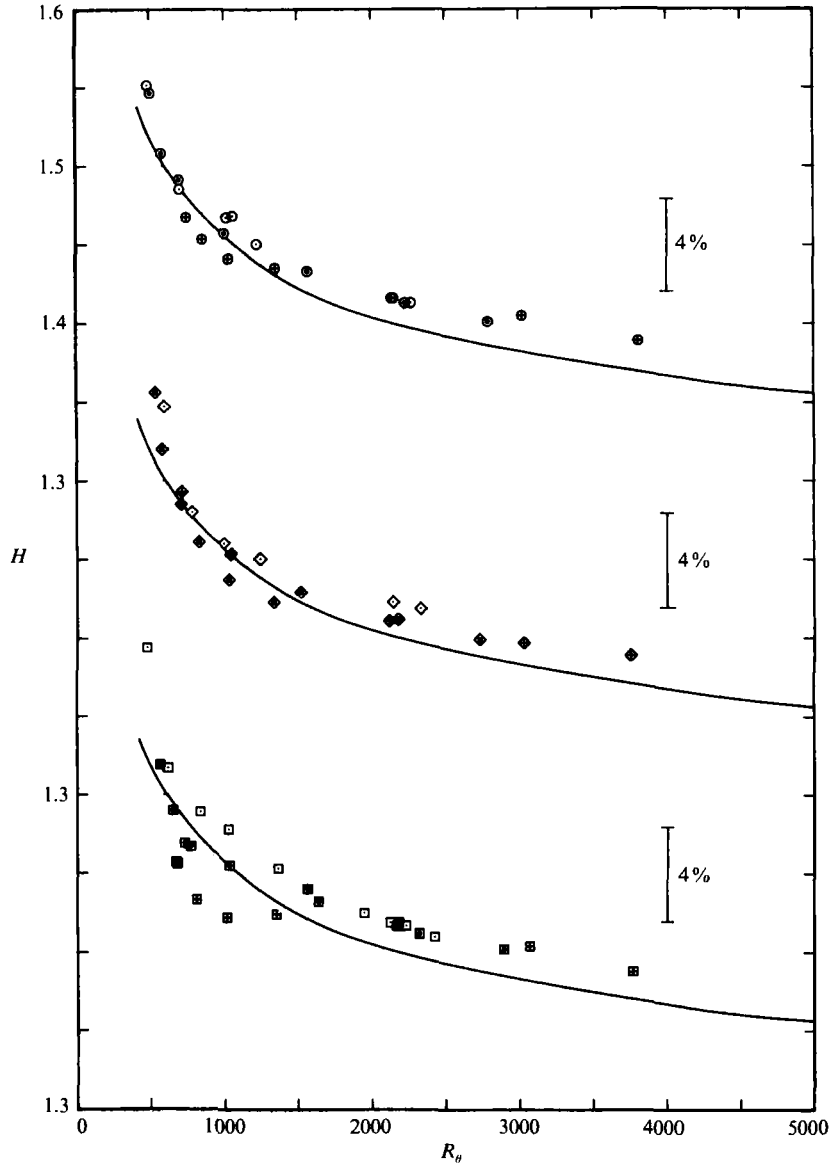

FIGURE 4. Variation of H with R_θ. Note shift in ordinate. ——, Coles' (1962) curve. For explanation of symbols see figure 2.

velocity of 14.0 m/s was actually chosen since this velocity was the maximum used in the range and consequently gave the greatest amount of overstimulation.

To verify the above technique it is necessary to compare current ΔU^+ data with Coles' (1962) curve as well as check the balances of momentum. Figure 2 shows data for the three devices compared with the curve of Coles and it can be seen that in all cases the under- and overstimulated data differ noticeably from the design data, whereas for the design flows, all three devices have approximately the same curve and these show good agreement with the curve of Coles. In addition, the balances of momentum for these nine flows have been shown by Erm (1988) to be acceptable.

When the current data were compared with Coles' curve, the method of determining ΔU^+ was the same as that used by Coles.

The above strongly suggests that the empirical technique is in fact valid, at least for the limited amount of data presented here, but as further confirmation the current data were compared with other low-Reynolds-number flow characteristics published by Coles (1962) to check on possible differences.

Figure 3 shows current data for the three devices compared with Coles' curve of C_f *vs.* $C_f R_\theta$. The data for the nine flow cases agree well with the curve at the higher values of R_θ, but there are some departures at the lower values of R_θ. For these lower values of R_θ, the design flows generally show good agreement with the curve, except perhaps for the pins where some discrepancies do occur. The data for the design flows clearly exhibit a better overall agreement with the curve than do the data for corresponding overstimulated flows and the overall agreement with the curve for the design flows is about the same as for the understimulated flows. At the lowest values of R_θ, data points often deviate noticeably below the curve and these data points correspond to the data points on figure 2 that show sharp rises in the values of ΔU^+.

The values of H for the three devices are shown in figure 4 where they are compared with Coles' curve. For all three devices, the degree of stimulation has more effect on the value of H at low values of R_θ than it does at high values, which is consistent with earlier trends. The data for the design flows agree with Coles' curve better than do the data for the under- and overstimulated flows, except perhaps for the wire, where the design flow and the understimulated flow show about the same agreement with the curve. Thus different amounts of stimulation, but for a given value of R_θ, can affect the shapes of the profiles. Although none of the data show a large variation from Coles' curve, as can be gauged from the tolerance bands included on figure 4, the design flows nevertheless give the best overall agreement with the curve.

From the above it can be seen that the current data for C_f and H further support the validity of the empirical technique described above for obtaining correctly stimulated flows.

Since the above design flows for the three devices had acceptable low-Reynolds-number behaviour and satisfied momentum balance requirements they were used for further mean-flow and turbulence measurements. Additional mean-flow and turbulence measurements were also taken for the three devices for the off-design flows to study the effects on the flows of under- and overstimulation.

4. Analysis of mean-flow results

Mean-flow data associated with the initial stages of this investigation, which may not be included in this paper, have been presented by Erm, Smits & Joubert (1987). Some of these data have been used by Spalart (1988) when he checked his numerical predictions for low-Reynolds-number flows.

4.1. $\Delta U/U_\tau$ *vs.* R_θ *relationships*

The ΔU^+ plots shown in figure 2 indicate that, for each device, the three curves associated with nominal reference velocities of 8.0, 10.0 and 14.0 m/s often differ noticeably at the lower values of R_θ, but there is a general tendency for the three curves to merge together by about $R_\theta = 2500$ to 3000. For a change in the velocity from 8.0 to 14.0 m/s for all devices, the amount of variation in the curves is greatest for the pins. Thus on the basis of the ΔU^+ curves, the wire and grit are less sensitive to changes in velocity than the pins, but it must be pointed out that the opposite

Group	R_θ from mean-flow profiles	Nominal reference velocity (m/s)	Tripping device	x (m)	δ (m)	ν/U_τ $\times 10^5$ (m)	Broadband turbulence profiles	Spectral measure-ments
1	697	10.0	Wire	0.260	0.0099	3.084	*u uv uw*	*u v w*
	706	10.0	Grit	0.260	0.0101	3.082	*u uv uw*	*u v w*
	729	10.0	Pins	0.220	0.0110	3.065	*u uv uw*	*u v w*
	mid pt. = 713 Var'n = ±2.2%							
2	1017	8.0	Wire	0.660	0.0175	4.119	*u*	*u*
	997	8.0	Grit	0.700	0.0174	4.069	*u*	*u*
	1024	8.0	Pins	0.580	0.0168	4.124	*u*	*u*
	1003	10.0	Wire	0.440	0.0139	3.245	*u uv uw*	*u v w*
	1042	10.0	Grit	0.460	0.0145	3.271	*u uv uw*	*u v w*
	1027	10.0	Pins	0.420	0.0141	3.241	*u uv uw*	*u v w*
	1033	14.0	Wire	0.260	0.0106	2.307	*u*	*u*
	1029	14.0	Grit	0.260	0.0105	2.289	*u*	*u*
	1013	14.0	Pins	0.260	0.0107	2.254	*u*	*u*
	mid pt. = 1020 Var'n = ±2.2%							
3	1568	10.0	Wire	0.900	0.0210	3.461	*u uv uw*	*u v w*
	1520	10.0	Grit	0.900	0.0206	3.425	*u uv uw*	*u v w*
	1565	10.0	Pins	0.820	0.0203	3.476	*u uv uw*	*u v w*
	mid pt. = 1544 Var'n = ±1.6%							
4	2151	8.0	Wire	1.860	0.0358	4.522	*u*	*u*
	2146	8.0	Grit	1.780	0.0351	4.556	*u*	*u*
	2230	8.0	Pins	1.780	0.0368	4.570	*u*	*u*
	2226	10.0	Wire	1.460	0.0293	3.617	*u uv uw*	*u v w*
	2178	10.0	Grit	1.460	0.0286	3.590	*u uv uw*	*u v w*
	2181	10.0	Pins	1.340	0.0286	3.638	*u uv uw*	*u v w*
	2137	14.0	Wire	0.900	0.0201	2.565	*u*	*u*
	2119	14.0	Grit	0.900	0.0203	2.551	*u*	*u*
	2169	14.0	Pins	0.900	0.0202	2.571	*u*	*u*
	mid pt. = 2175 Var'n = ±2.6%							
5	2788	10.0	Wire	1.940	0.0367	3.792	*u uv uw*	*u v w*
	2730	10.0	Grit	1.940	0.0360	3.693	*u uv uw*	*u v w*
	2889	10.0	Pins	1.940	0.0375	3.730	*u uv uw*	*u v w*
	mid pt. = 2810 Var'n = ±2.8%							

TABLE 2. Details of mean-flow profiles, broadband-turbulence profiles and spectra

trend applies when the devices are compared on the basis of their C_f distributions shown in figure 1. An interesting feature of most of the curves shown in figure 2 is their unusual behaviour at their left-hand extremities where they turn around and have the opposite trend to Coles' curve. This phenomenon has also been noticed by Purtell *et al.* (1981). All of the plotted points on figure 2 in the regions of the reversals of the curves were computed for layers that had become turbulent, as will be explained in §4.3 for the design flow for the grit, so therefore the flows in this region are definitely low-Reynolds-number turbulent boundary-layer flows and are thus worthy of being studied.

The fact that the curves for the design flows for the three devices show good agreement with Coles' curve means that, whenever the design flows are compared to see whether the type of device used affects other mean-flow behaviour or turbulence behaviour, then the comparisons can be made on a sound basis.

4.2. *Constant values of R_θ for comparison between different flows*

In order that the mean-flow characteristics of any of the above nine flows could be systematically compared to each other, it was essential that mean-flow profiles were taken in each flow for values of R_θ close to those at which the comparisons were to be made. Twenty seven mean-flow profiles corresponding to five different ranges of values of R_θ were taken and details of these profiles are given in table 2. As can be seen, the midpoint values of R_θ for groups 1 to 5 are respectively 713, 1020, 1544, 2175 and 2810. For the three design flows, profiles were associated with each of these five nominal values of R_θ, while for the three understimulated and the three overstimulated flows, profiles were associated with nominal values of R_θ of 1020 and 2175.

The mean-flow experimental programme summarized in table 2 formed the basis for the broadband-turbulence and spectral experimental programmes. Details of the turbulence measurements are also given in this table. u-broadband-turbulence profiles and u-spectra were taken for each of the twenty seven cases but uv- and uw-broadband-turbulence profiles and v- and w-spectra were limited to the design flows.

By appropriately selecting measurements referred to in table 2, it was possible to compare the different flows in such a manner that the effects of R_θ, tripping device and different amounts of stimulation, each considered independently, could be determined.

4.3. *Velocity profiles for correctly stimulated flows*

Mean-flow velocity profiles for the wire for the design flow and for different values of R_θ are shown plotted in figure 5. Values of y/δ corresponding to the end of the logarithmic region are shown. To assess the effects on the profiles of variation in R_θ for each of the three devices, it is necessary to plot the profiles as shown in figure 6. Likewise, to assess the effects on the profiles of variations of device at each of the five nominal values of R_θ, it is necessary to plot the profiles as shown in figure 7.

As expected, figure 6 indicates that, for each of the three devices, the data in the wall region collapse, but the data in the outer region depend strongly on R_θ. Figure 7 indicates that for all nominal values of R_θ, except perhaps the lowest, i.e. $R_\theta \approx 713$, the type of device used has only a very minor effect upon the profiles when they are plotted using these coordinates. In figure 7 it may be necessary to interpret the symbols of the collapsed profiles in the context of figures 5 and 6.

The data contained in figures 6 and 7 were replotted as shown in figures 8 and 9 respectively. As expected, figure 8 clearly shows that for each of the devices, the velocity-defect profiles are not universal at low values of R_θ but change monotonically with R_θ. In each case, there is a tendency for the profiles to converge at the higher values of R_θ. Figure 9 indicates that for all nominal values of R_θ, except perhaps $R_\theta \approx 713$, the type of device used does not greatly affect the profiles.

A mean-flow profile for the grit for the design flow, corresponding to $R_\theta = 537$ and $x = 0.140$ m, is shown in figure 10. For comparison purposes, data for the grit from figure 6 have been replotted on figure 10. The outer flow region of the profile for $R_\theta = 537$ has a different form compared with profiles having higher values of R_θ, and the reason for the increased values of ΔU^+ shown in figure 2 now becomes apparent. The flow corresponding to $R_\theta = 537$ exhibits characteristics of turbulence, namely a

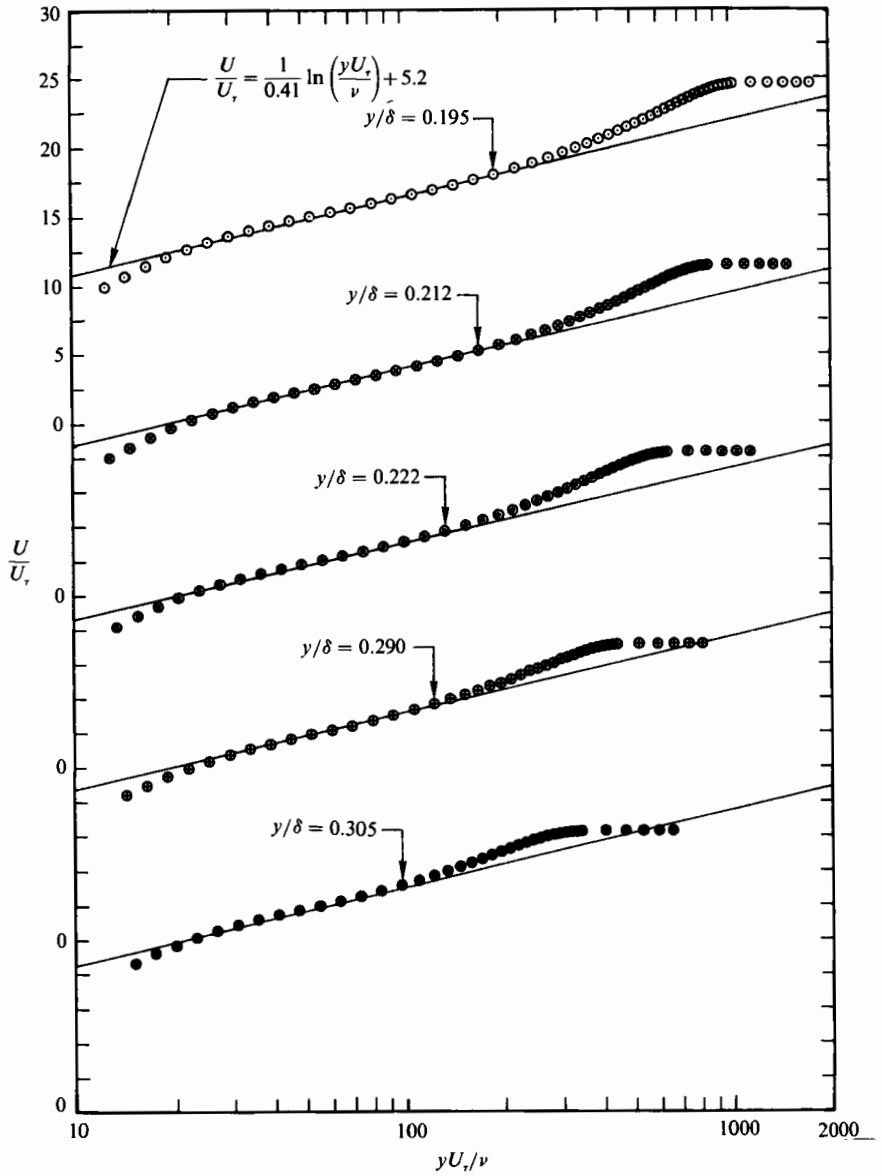

FIGURE 5. Mean-flow velocity profiles for wire for design flow. Note shift in ordinate. ●, $R_\theta = 697$; ⊕, 1003; ⊙, 1568; ⊗, 2226; ⊙, 2788.

linear logarithmic region on the profile shown in figure 10 and also the Preston-tube values of C_f correspond to turbulent flow, as shown in figure 1.

The logarithmic region was found to diminish with R_θ as shown in figure 5. Logarithmic regions were found to be present for all values of R_θ, provided the flow was turbulent, and the lowest value of R_θ at which a logarithmic region was observed for a design-flow profile whose value of ΔU^+ was close to Coles' (1962) curve, was $R_\theta = 581$. The profile was for the wire. The extreme design-flow profile for the grit, shown in figure 10, displayed a logarithmic region down to $R_\theta = 537$, but this profile had an unusual form for the wake as explained above. Such a profile for the wire displayed a logarithmic region down to $R_\theta = 509$.

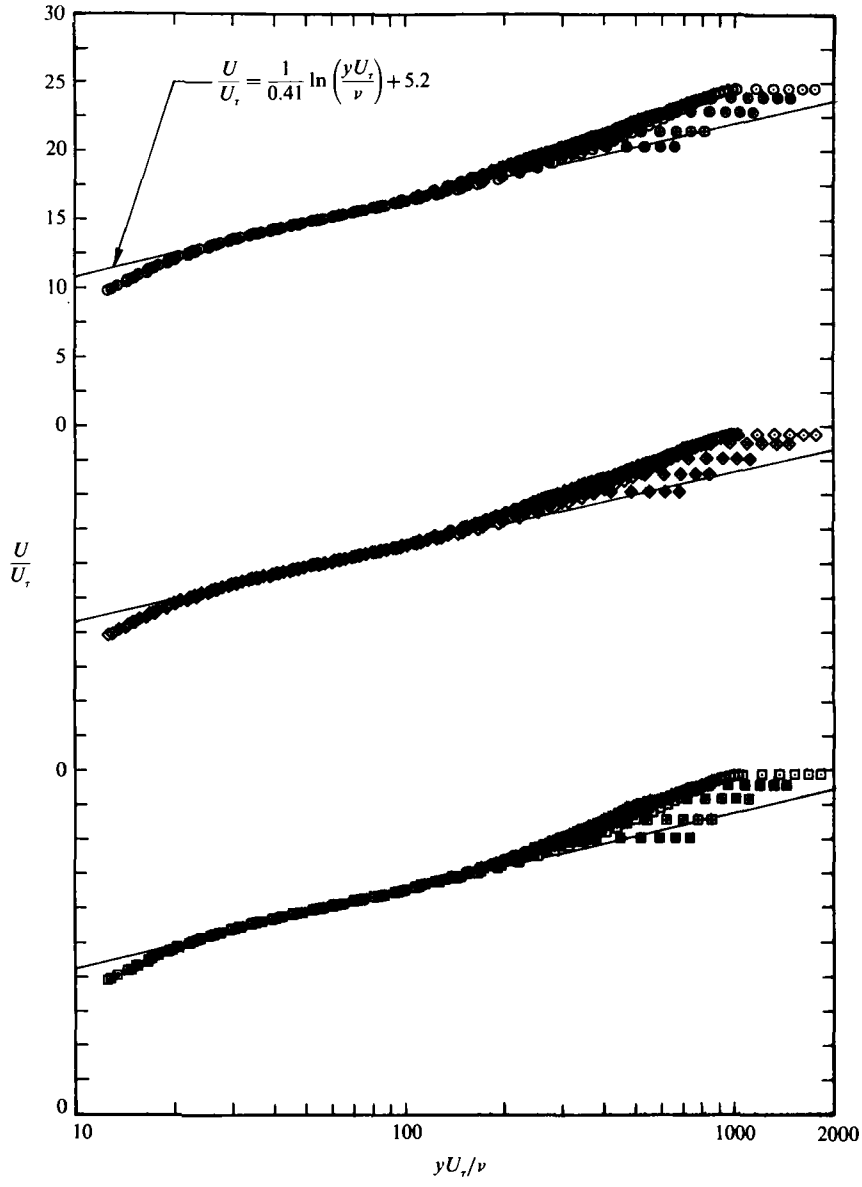

FIGURE 6. Mean-flow velocity profiles for design flows showing effects of R_θ for three devices. Note shift in ordinate. Wire: ●, $R_\theta = 697$; ⊕, 1003; ⊙, 1568; ⊗, 2226; ⊙, 2788. Grit: ◆, $R_\theta = 706$; ⊕, 1042; ◈, 1520; ⊗, 2178; ◇, 2730. Pins: ■, $R_\theta = 729$; ⊞, 1027; ▣, 1565; ⊠, 2181; ⊡, 2889.

4.4. *Velocity profiles for under- and overstimulated flows*

Profiles used to determine the effects of under- and overstimulation for each of the devices are shown in figures 11 and 12 for $R_\theta \approx 1020$ and $R_\theta \approx 2175$ respectively. The profiles for $R_\theta \approx 1020$ are affected by the degree of stimulation, but the differences are only convincing for the pins. Any differences in the profiles for $R_\theta \approx 2175$ are negligible. Although the differences within a group of profiles for $R_\theta \approx 1020$ are often within the experimental uncertainty of the measurements, the trends of the data suggest that real differences can exist in profiles having approximately the same

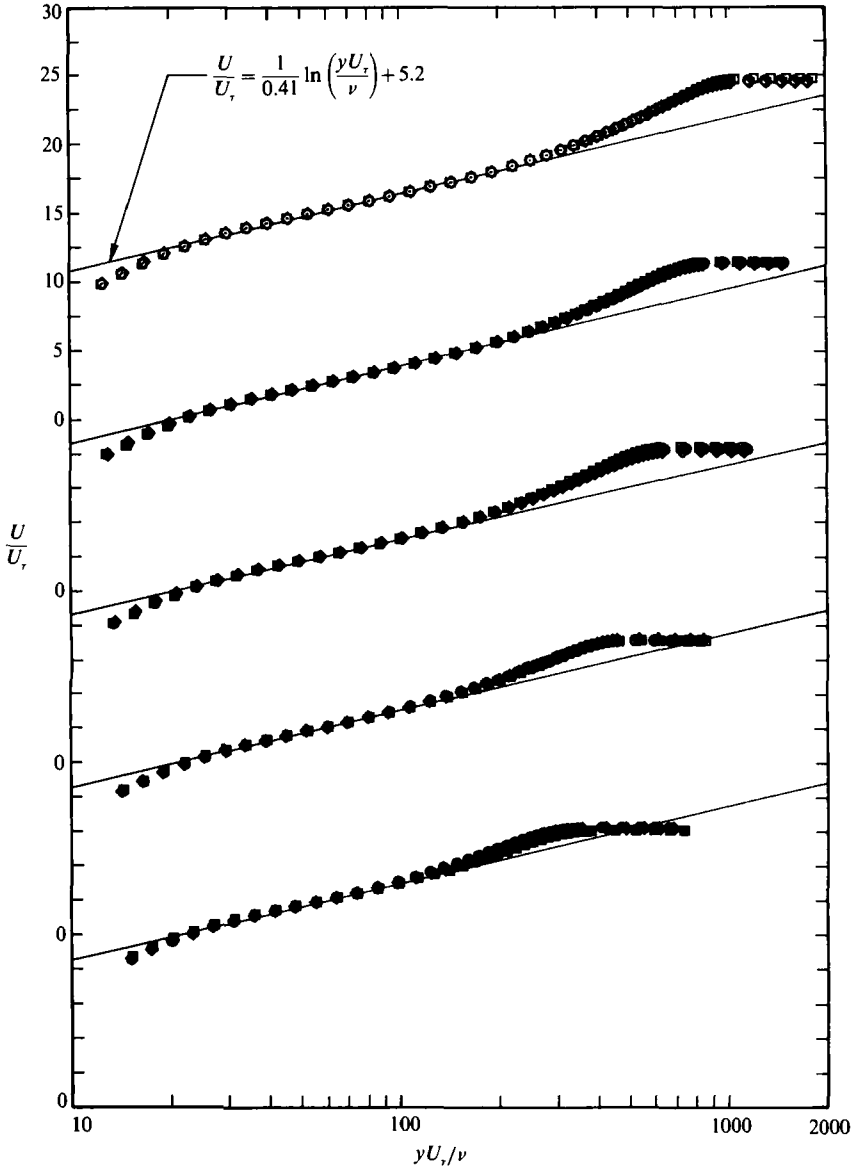

FIGURE 7. Mean-flow velocity profiles for design flows showing effects of device for five nominal values of R_θ. Note shift in ordinate. For explanation of symbols see figure 6.

value of R_θ, but different amounts of stimulation. It will be recalled that Purtell (1978) and Smits *et al.* (1983) did not take any account of how parameters were affected by the degree of stimulation.

4.5. *Skin-friction coefficients*

Transverse C_f measurements for the design flows were taken with a Preston tube for the three devices for different values of R_θ. The measurements were spaced at intervals of 4.5 mm and extended 108 mm along both sides of the wind-tunnel centreline so that they covered approximately the central third of the smooth wall.

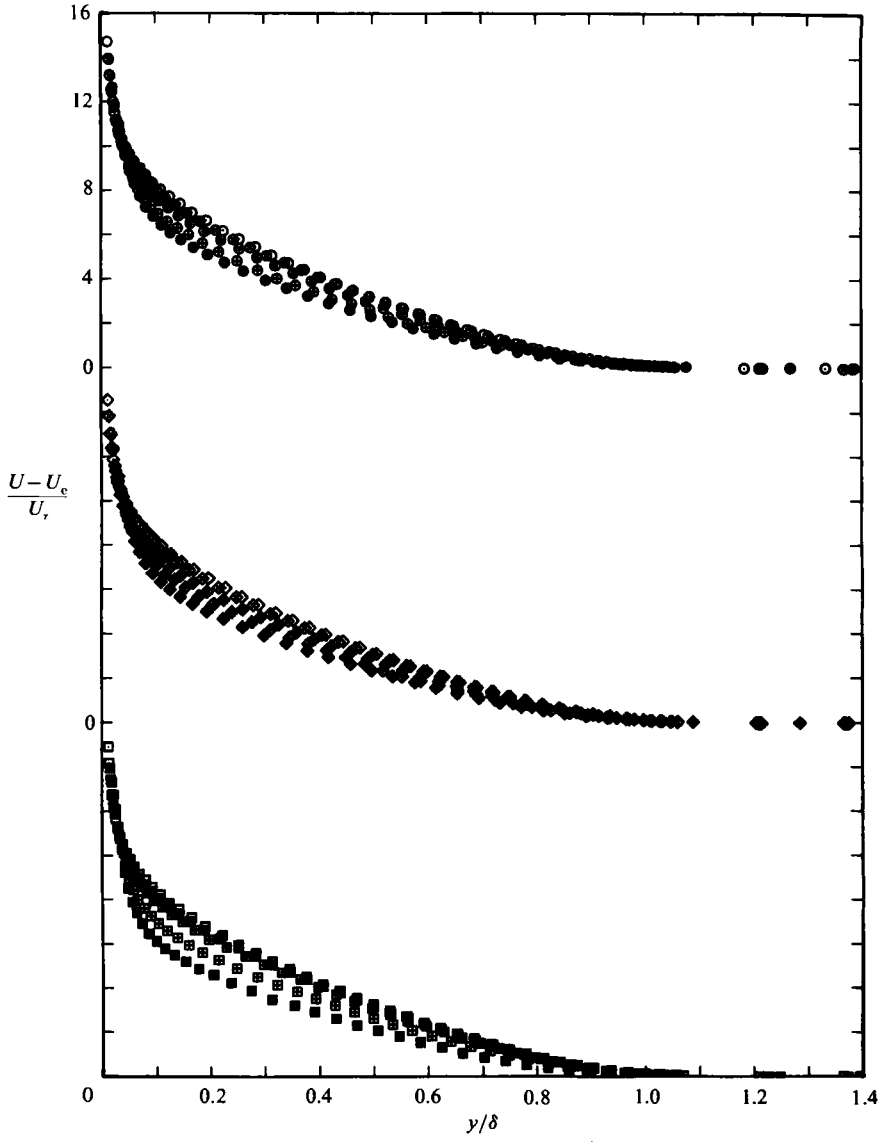

FIGURE 8. Mean-flow velocity-defect profiles for design flows showing effects of R_θ for three devices. Note shift in ordinate. For explanation of symbols see figure 6.

The above spacing was chosen so that measurements would be taken at locations both directly behind the pins and also halfway between these. Values of C_f were normalized by C_{f_m}, the mean value of C_f within a particular set, and values of C_f/C_{fm} are shown plotted against z in figure 13. The actual experimental points are shown and, as an aid to interpreting the results, the experimental points have been joined by straight lines. The grid marks on the abscissa correspond to pin locations.

For each device, the normalized values of C_f fluctuate the most rapidly with z at the lower values of R_θ, but the fluctuations become less pronounced with increasing R_θ. Also, the overall range of variation is greatest at the lower values of R_θ, except perhaps for the wire, where the range of variation does not change much for changes in R_θ. The above behaviour is particularly noticeable for the pins. For this device, the

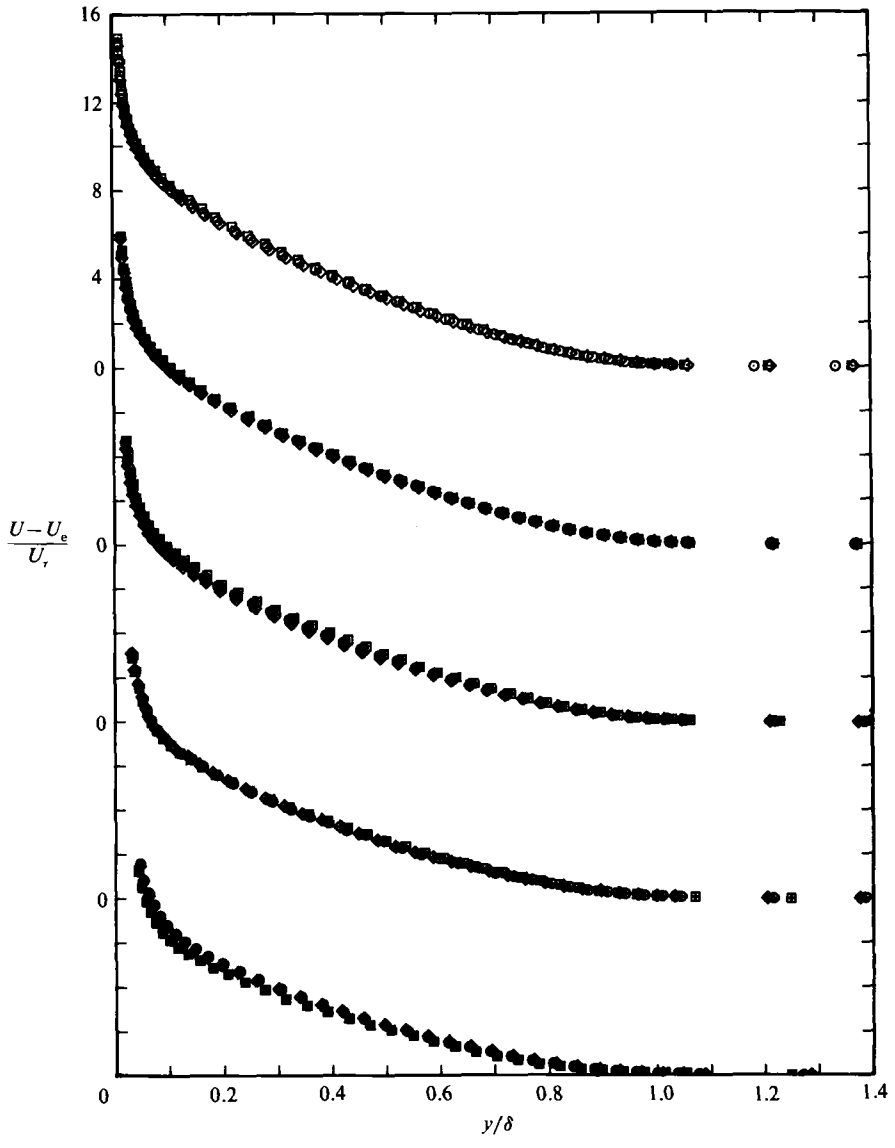

FIGURE 9. Mean-flow velocity-defect profiles for design flows showing effects of device for five nominal values of R_θ. Note shift in ordinate. For explanation of symbols see figure 6.

peaks and valleys show a strong correlation with pin position for $R_\theta = 770$, but the correlation disappears as the flow develops. The behaviour is undoubtedly related to the fact that wedges of turbulent flow form behind the pins. There does not seem to be any pattern in the transverse distributions for the wire and the grit.

A notable feature of figure 13 is that the data for the three devices, although dissimilar in the early stages of development, show some remarkable similarities for $R_\theta \approx 2175$ and above. In this region the peaks and valleys for the three devices show similar behaviour in corresponding cases and the type of device used clearly now has little influence on the transverse distributions. The perturbations that remain are most likely a consequence of the characteristics of the wind tunnel itself.

It will be recalled from figure 1 that the longitudinal C_f distributions for the pins

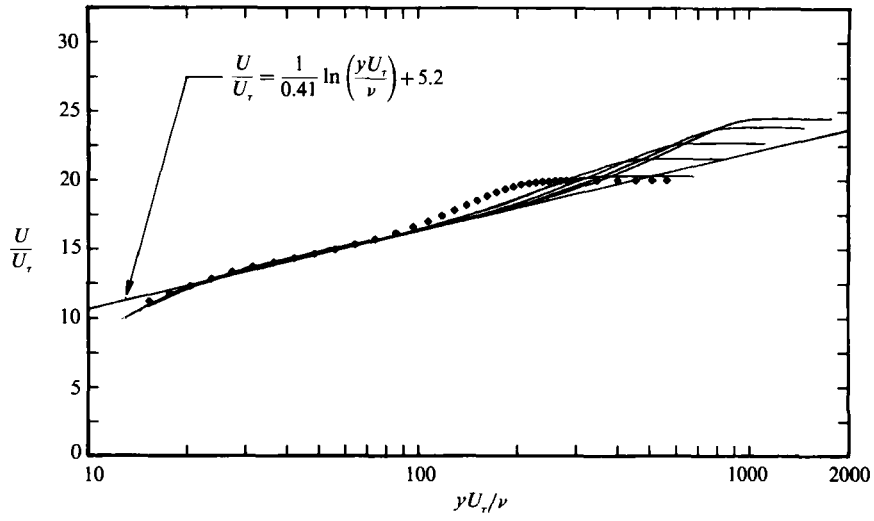

FIGURE 10. Mean-flow velocity profiles for various values of R_θ for design flow for grit. ◆, $R_\theta = 537$, $x = 0.14$ m; ——, various R_θ, based on figure 6.

displayed unusual behaviour for a nominal velocity of 9.0 m/s. From figure 13 it can be seen that this could be due to lateral variations in C_f.

5. Analysis of broadband-turbulence results

Erm (1988) compared mean velocities from a single-wire probe with those from a Pitot probe and also compared $(\overline{u^2})^{\frac{1}{2}}/U_\tau$ profiles from the single-wire probe with those from the crossed-wire probe in both *uv*- and *uw*-modes. In all cases the agreement was excellent which is encouraging and gives some credibility to the results.

5.1. *Broadband-turbulence characteristics for correctly stimulated flows*

The plots to be presented for the broadband-turbulence data will not correspond exactly to the format of those presented for mean-flow data, but instead will be abridged. Plots showing how a quantity varies with R_θ will correspond to five values of R_θ, but only for the wire. Plots showing how a quantity depends upon the device used will be for the three devices for five nominal values of R_θ, but only for one of the measurements of that type, e.g. $\overline{v^3}$ triple products will be used to represent all types of triple products. The plots given will be representative of the range of plots. This approach significantly simplifies the presentation of data, while still conveying most of the desired information. The unabridged plots are given by Erm (1988).

5.1.1. *Reynolds stresses*

Profiles of $\overline{u^2}$, $\overline{v^2}$, $\overline{w^2}$ and $-\overline{uv}$, scaled by U_e^2, for the wire for different values of R_θ are shown in figure 14(*a–d*). With this scaling, the Reynolds-stress profiles depend on R_θ, but the extent of the dependency varies throughout the y/δ range. The variation of the profiles with R_θ is greatest near the wall, but diminishes with increasing y/δ. Since the wall region was found to extend to $y/\delta \approx 0.31$ for $R_\theta = 697$ and to $y/\delta \approx 0.20$ for $R_\theta = 2788$, the effects of R_θ are most pronounced in the wall region or slightly beyond. The profiles for the different Reynolds stresses show monotonic trends with

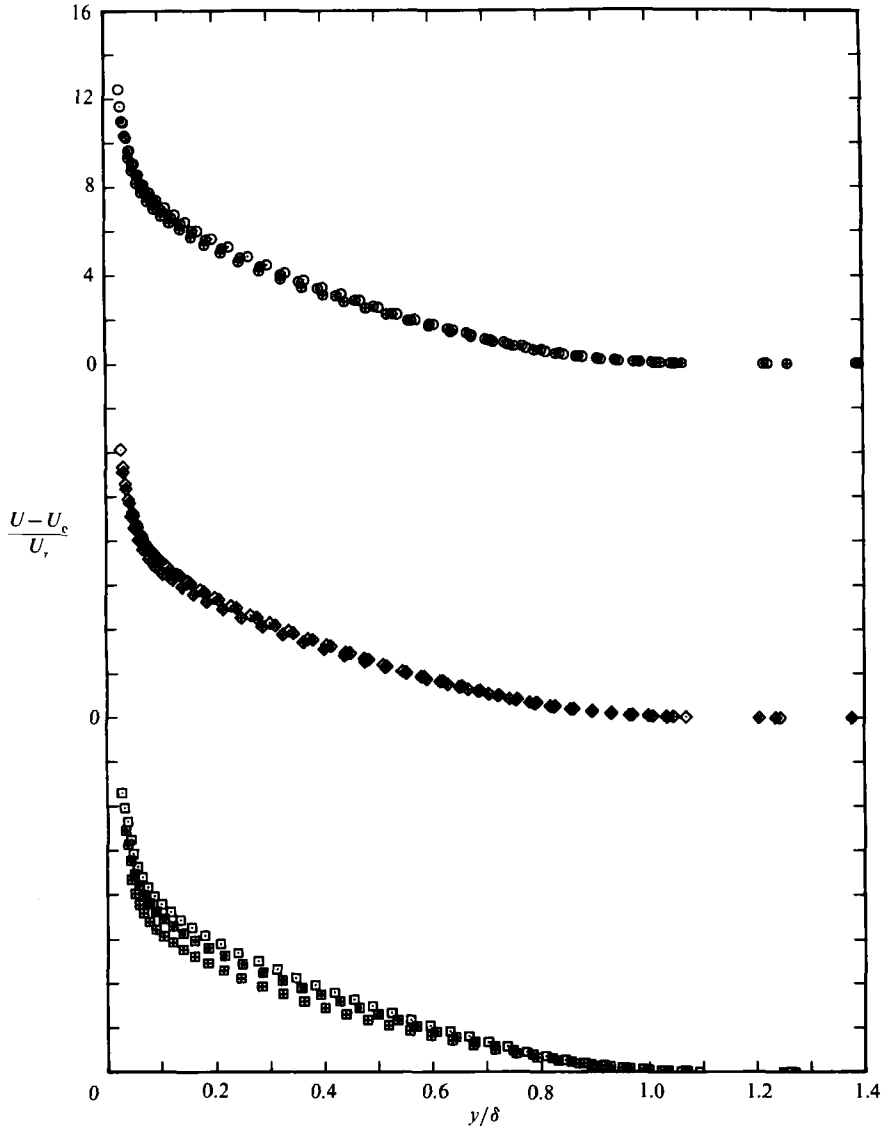

FIGURE 11. Mean-flow velocity profiles for three devices showing effects of different amounts of stimulation. Note shift in ordinate. Velocities given below are nominal values. Wire: ⊙, 8.0 m/s, $R_\theta = 1017$; ⊙, 10.0, 1003; ⊕, 14.0, 1033. Grit: ◇, 8.0 m/s, $R_\theta = 997$; ◈, 10.0, 1042; ⊕, 14.0, 1029. Pins: ⊡, 8.0 m/s, $R_\theta = 1024$; ▣, 10.0, 1027; ⊞, 14.0, 1013.

R_θ, although in some cases the differences between the profiles for $R_\theta = 2226$ and 2788 are quite small.

Profiles of $\overline{v^3}/U_e^3$ for the three devices for five nominal values of R_θ are shown in figure 15 to indicate the dependency of Reynolds stresses upon device over the R_θ range. With this scaling, the profiles for the three devices clearly do not agree at $R_\theta \approx 713$, but for $R_\theta \approx 1020$ and above, the type of device used has only a small or negligible effect on the profiles.

Profiles of $(\overline{u^2})^{\frac{1}{2}}/U_\tau$ *vs.* $\log y^+$ are shown in figure 16. With this scaling, the profiles are strongly Reynolds-number dependent and there is no obvious collapse of the data

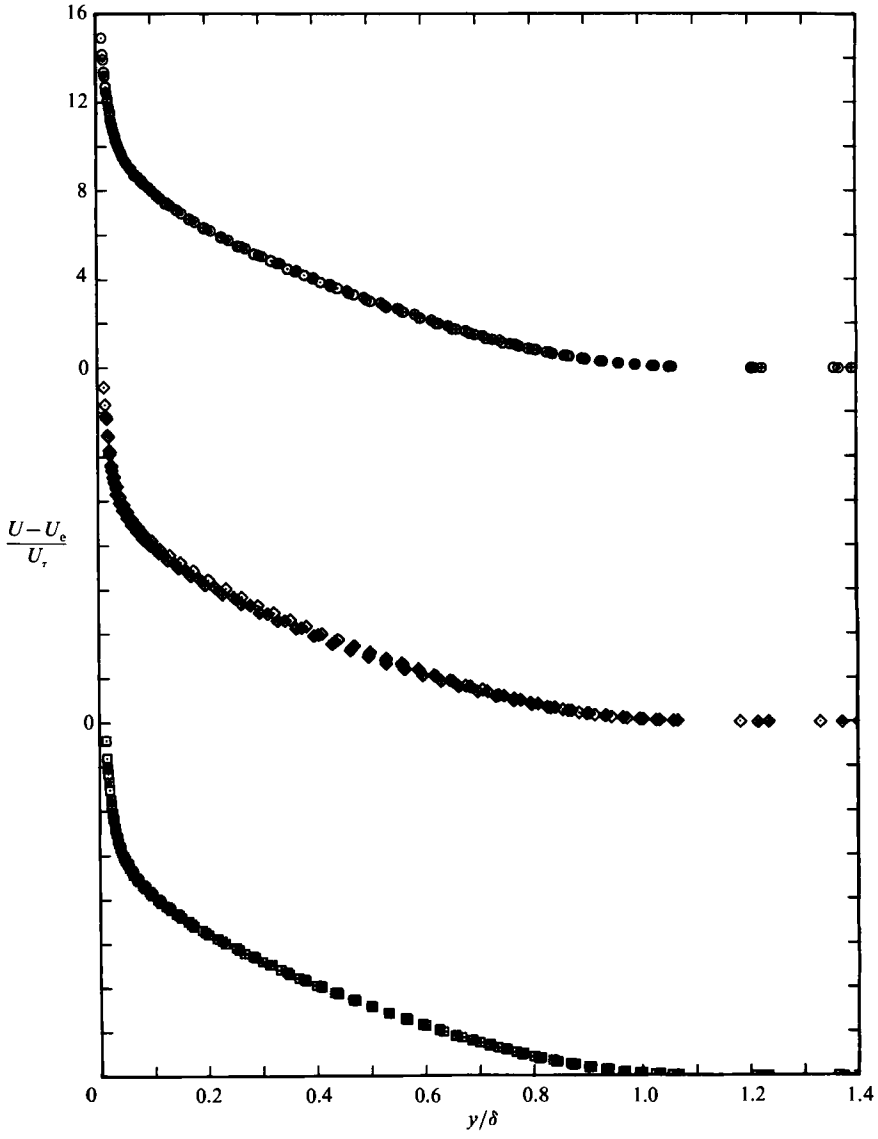

FIGURE 12. Mean-flow velocity profiles for three devices showing effects of different amounts of stimulation. Note shift in ordinate. Velocities given below are nominal values. Wire: ⊙, 8.0 m/s, $R_\theta = 2151$; ⊙, 10.0, 2226; ⊕, 14.0, 2137. Grit: ◇, 8.0 m/s, $R_\theta = 2146$; ◈, 10.0, 2178; ⊕, 14.0, 2119. Pins: ⊡, 8.0 m/s, $R_\theta = 2230$; ▣, 10.0, 2181; ⊞, 14.0, 2169.

for any of the values of y^+ shown. There is a possibility, however, that near the wall, the decreases in the magnitudes of $(\overline{u^2})^{\frac{1}{2}}/U_\tau$ with decreasing R_θ may be influenced by the spatial resolution capabilities of the single hot-wire sensor having length, l, and diameter, d. Ligrani & Bradshaw (1987) took $(\overline{u^2})^{\frac{1}{2}}$ measurements in low-Reynolds-number flows ($R_\theta = 2620$ for most of their measurements) using single-wire probes having sensors of different lengths and diameters and found that, in the viscous sublayer, as the value of $l^+ \equiv lU_\tau/\nu$ increased above 20–25, the measured values of $(\overline{u^2})^{\frac{1}{2}}$ decreased significantly and abruptly. This was found to be most evident for $8 < y^+ < 17.5$. They also found that for l^+ less than 20–25, the measured values of $(\overline{u^2})^{\frac{1}{2}}$

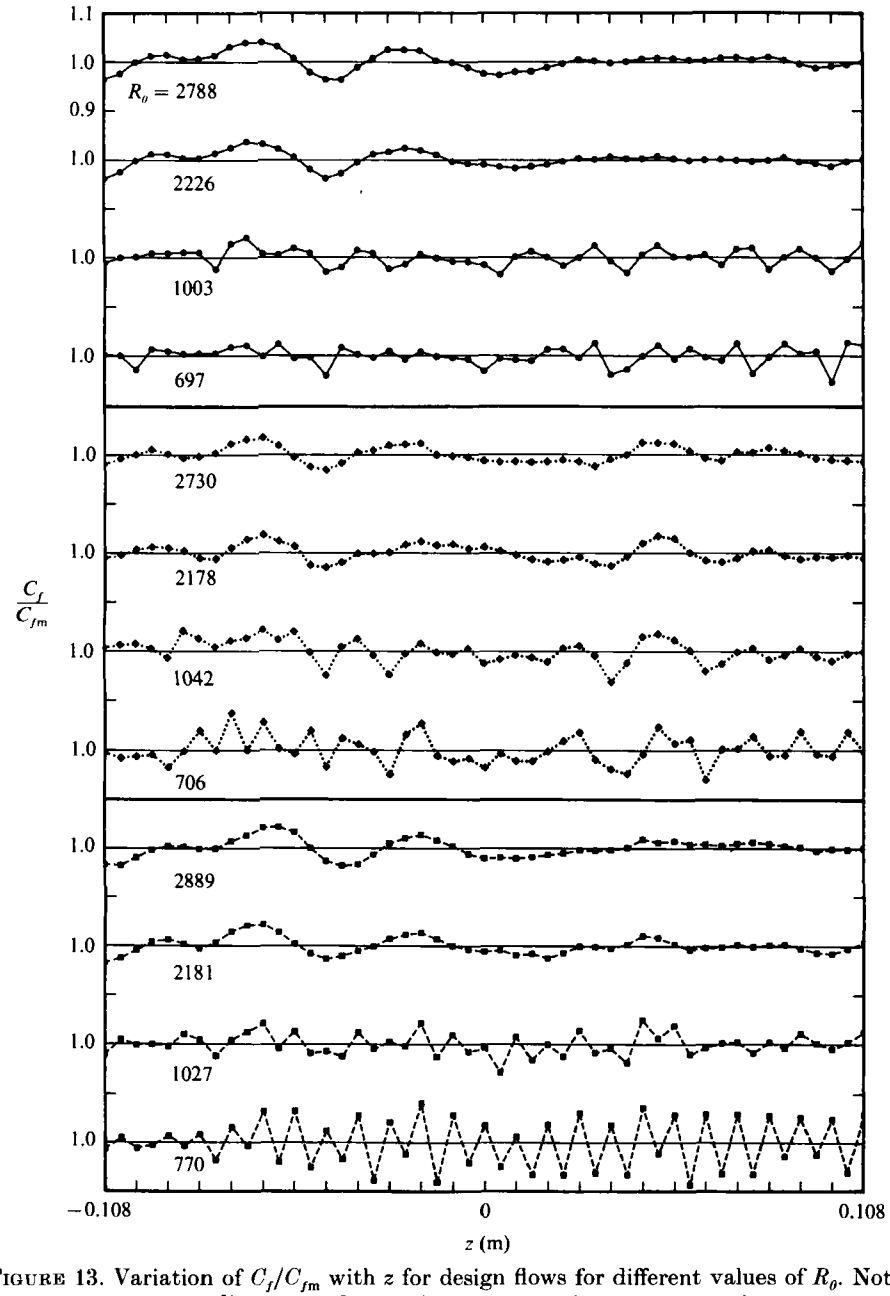

FIGURE 13. Variation of C_f/C_{fm} with z for design flows for different values of R_θ. Note shift in ordinate: —●—, wire; ···◆···, grit; ---■---, pins.

changed less than 4%, increasing slightly as l^+ decreased. The l/d ratio of the sensor was also found to influence their results and they concluded that adequately accurate results for the longitudinal velocity fluctuations near the wall can be obtained if $l^+ < 20$ and $l/d > 200$. They also found that attenuation for a given sensor became less severe as y^+ increased. The sensor used to obtain the data in figure 16 had $l/d = 180$, $l^+ = 29.3$ for $R_\theta = 697$ and $l^+ = 24.2$ for $R_\theta = 2788$. Although these values of l/d and l^+ do not quite satisfy the conditions of Ligrani & Bradshaw, there is nevertheless

reasonably close agreement. Furthermore, there are very few points on the profiles having $8 < y^+ < 17.5$, where attenuation is most evident. Thus, it is reasonable to conclude that the effects of spatial resolution on the profiles in figure 16 are most likely small.

The crossed-wire sensors had $l/d = 160$, $l^+ = 25.9$ for $R_\theta = 697$ and $l^+ = 21.4$ for $R_\theta = 2788$. These values of l^+ are comparable with those of Murlis *et al.* (1982), who quote $l^+ \approx 30$ for their crossed-wire probe. Possible attenuation of the crossed-wire measurements is a less important consideration compared with the single-wire measurements, since the former could not be taken as close to the wall. The limiting crossed-wire measurements correspond to $y^+ = 63.8$ for $R_\theta = 697$ and $y^+ = 52.7$ for $R_\theta = 2788$.

It is of interest to compare the data of figure 16, for the turbulent wall region (see §6.2.1), with predictions given by Perry & Li (1990). They proposed that

$$\overline{u^2}/U_\tau^2 = 2.39 - 1.03 \ln (y/\delta_H) - V[y^+], \tag{3}$$

where δ_H is a layer thickness and $V[y^+]$ is a viscous correction term. Values of $(\overline{u^2})^{\frac{1}{2}}/U_\tau$ predicted by this equation are shown in figure 16 for different values of R_θ. Predictions for the turbulent wall region are shown as full lines and outside this region as broken lines. In these predictions, the 99.5 % boundary-layer thickness was used and $V[y^+]$ was determined using an expression given by Perry & Li, namely

$$V[y^+] = 5.58(y^+)^{-\frac{1}{2}} - 22.4(y^+)^{-1} + 22.0(y^+)^{-\frac{5}{4}} - 5.62(y^+)^{-2} + 1.27(y^+)^{-\frac{11}{4}},$$

which was based on the work of Kovasznay (1948). Predictions are not given for the turbulent wall region for $R_\theta = 697$, for reasons explained in §6.2.1. For $y^+ = 60$, the difference between their predictions and current measurements of $(\overline{u^2})^{\frac{1}{2}}/U_\tau$ is about 9 % for $R_\theta = 1003$ and about 6 % for $R_\theta = 2788$. This discrepancy is probably influenced by the fact that the theory of Perry & Li was not developed for low-Reynolds-number flows. The lowest R_θ of their experiments, used when formulating their theory, was in fact greater than the highest R_θ of the current experiments ($R_\theta = 2828$ compared with $R_\theta = 2788$).

Perry & Li carried out checks to investigate specific problems associated with the use of crossed-wire probes. Problems covered with thermal prong effects, excessive cone angles of the approaching velocity vectors and aerodynamic prong effects. The checks were done for a free-stream velocity of 10 m/s on a smooth wall and the results were presented as profiles of $\overline{v^2}$ measurements, which are most affected by hot-wire problems. The profiles for the different cases collapsed well, indicating that the above factors did not have a significant influence on their results for the flow conditions chosen. Perry & Li also found that at a free-stream velocity of 10 m/s, the spatial resolution corrections for all three components of the turbulence are small on smooth walls. Since the hot-wire probes (DISA 55P51), filaments, circuitry and techniques used in the current investigation were similar to those used by Perry & Li when performing checks, it is not unreasonable to extend their findings to the current results. Furthermore, some of the early results of the current investigation, given by Erm *et al.* (1987), have been used by Perry & Li as an example of acceptable data.

In the literature, $\overline{w^2}$ at low Reynolds numbers is often approximated using the expression $(\overline{w^2})^{\frac{1}{2}} = 0.5((\overline{u^2})^{\frac{1}{2}} + (\overline{v^2})^{\frac{1}{2}})$. Erm (1988) plotted data for the wire and showed that, at $y/\delta = 0.5$, the actual measured value of $\overline{w^2}$ was about 20 % smaller than that determined from the above approximation for $R_\theta = 1003$ and about 17 % smaller for $R_\theta = 2226$.

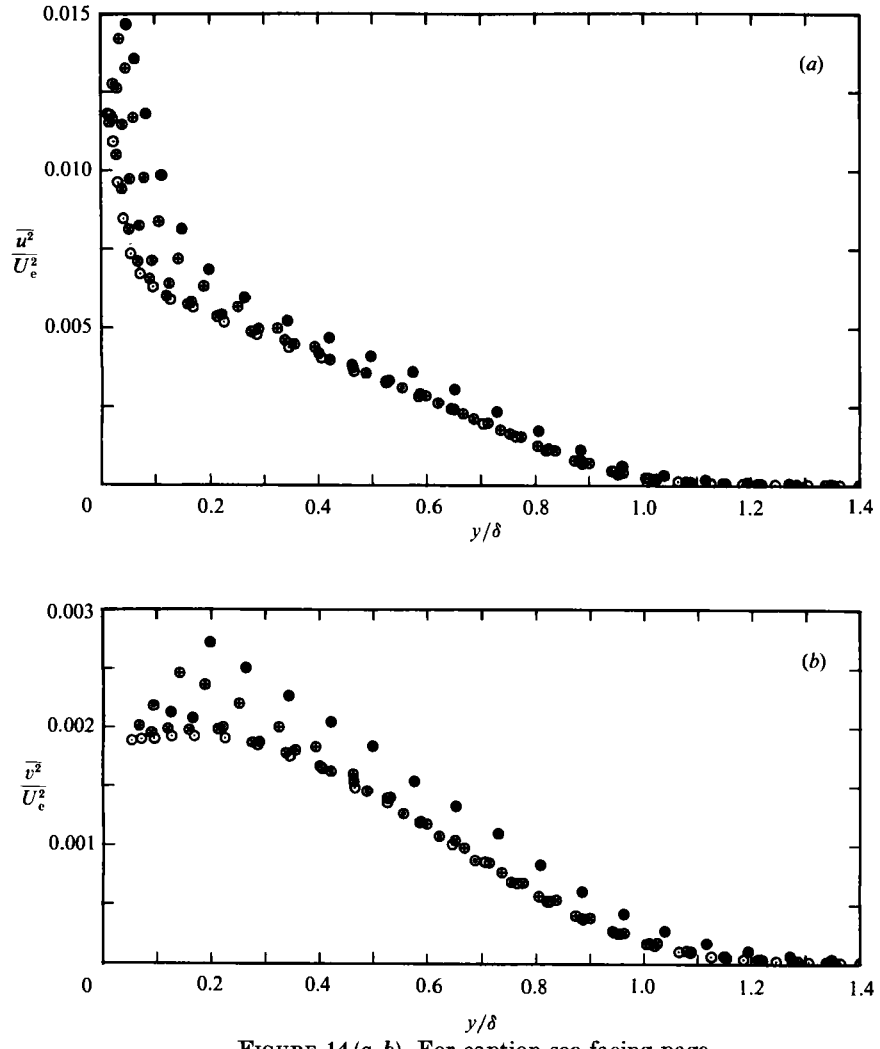

FIGURE 14(*a*, *b*). For caption see facing page.

5.1.2. *Triple products*

A good knowledge of the behaviour of triple products is of importance since they appear in the transport equations used for boundary-layer prediction methods. However, there is still a scarcity of reliable experimental data for low-Reynolds-number flows.

Profiles of $-\overline{u^3}$, $\overline{v^3}$, $\overline{u^2v}$ and $-\overline{uv^2}$, scaled by U_e^3, for the wire for different values of R_θ are shown in figure 17(*a–d*). As for the Reynolds stresses, the triple-product profiles depend on R_θ, but the dependency varies throughout the y/δ range and is greatest in the wall region or slightly beyond. Also, there is a general tendency for the profiles to vary monotonically with R_θ. A notable feature of figure 17(*a*) is the appearance of negative values of $-\overline{u^3}/U_e^3$ for low values of y/δ. These negative values of $-\overline{u^3}$ have also been reported in the literature by Barlow & Johnston (1988) ($R_\theta =$ 1140). Although their experiments were primarily concerned with the effects of concave curvature on turbulent-boundary-layer structure, some of their upstream

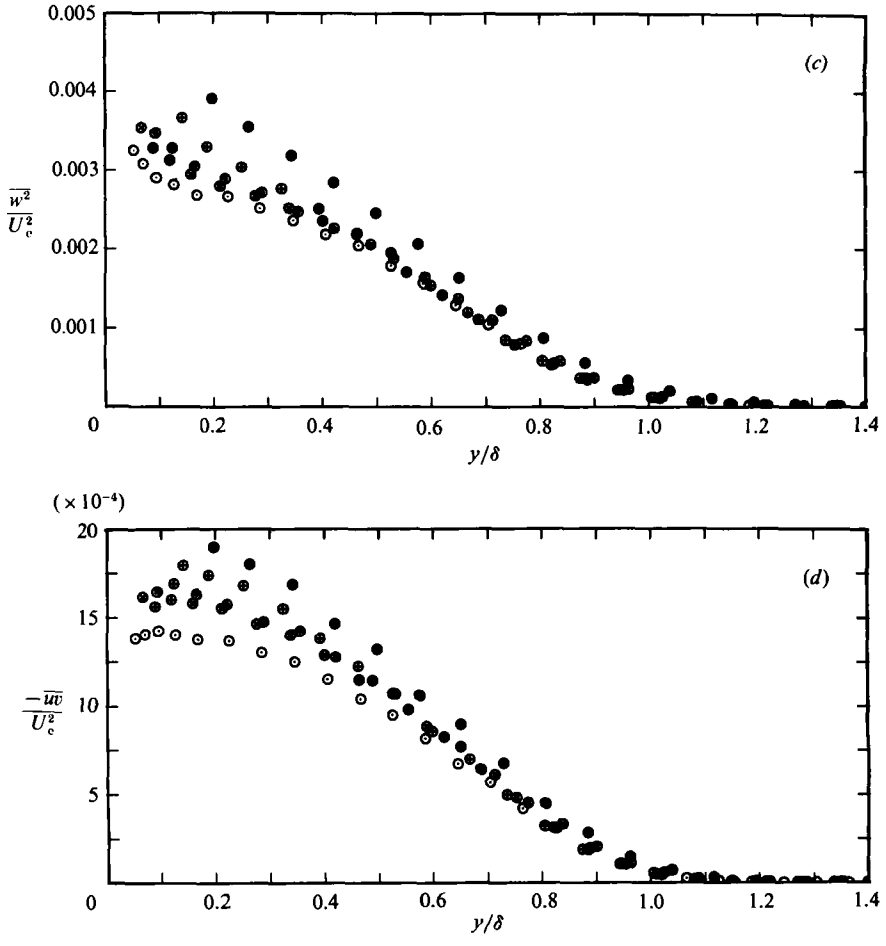

FIGURE 14. Profiles of Reynolds stresses for wire for design flow showing effects of R_θ. (*a*) $\overline{u^2}/U_e^2$; (*b*) $\overline{v^2}/U_e^2$; (*c*) $\overline{w^2}/U_e^2$; (*d*) $-\overline{uv}/U_e^2$. For explanation of symbols see figure 5.

measurements were taken before the start of the wall curvature. Since the other three types of triple products were taken with the crossed-wire probe, it was not possible to take measurements close enough to the wall to see if they changed sign in this region, but it is a matter of interest that Barlow & Johnston did in fact show this to be the case.

Profiles of $\overline{v^3}/U_e^3$ for the three devices for five nominal values of R_θ are shown in figure 18 to indicate the dependency of triple products on device over the R_θ range. The type of device used has a large effect upon the profiles for $R_\theta \approx 713$, and although the collapse of the profiles for $R_\theta \approx 1020$ and above is not quite as good as for the Reynolds-stress profiles, the type of device used does not have a significant effect on the triple-product profiles if allowances are made for the inevitable scatter that occurs with triple-product measurements.

Murlis *et al.* (1982) did not present data for values of y/δ less than about 0.2 for any of their triple-product profiles, and for some of these profiles the limiting value of y/δ is as high as about 0.4. Thus their data do not show the details of the peaks closest to the wall or indicate that profiles depend strongly on R_θ in this region. The current data for low values of y/δ are thus especially significant in this respect.

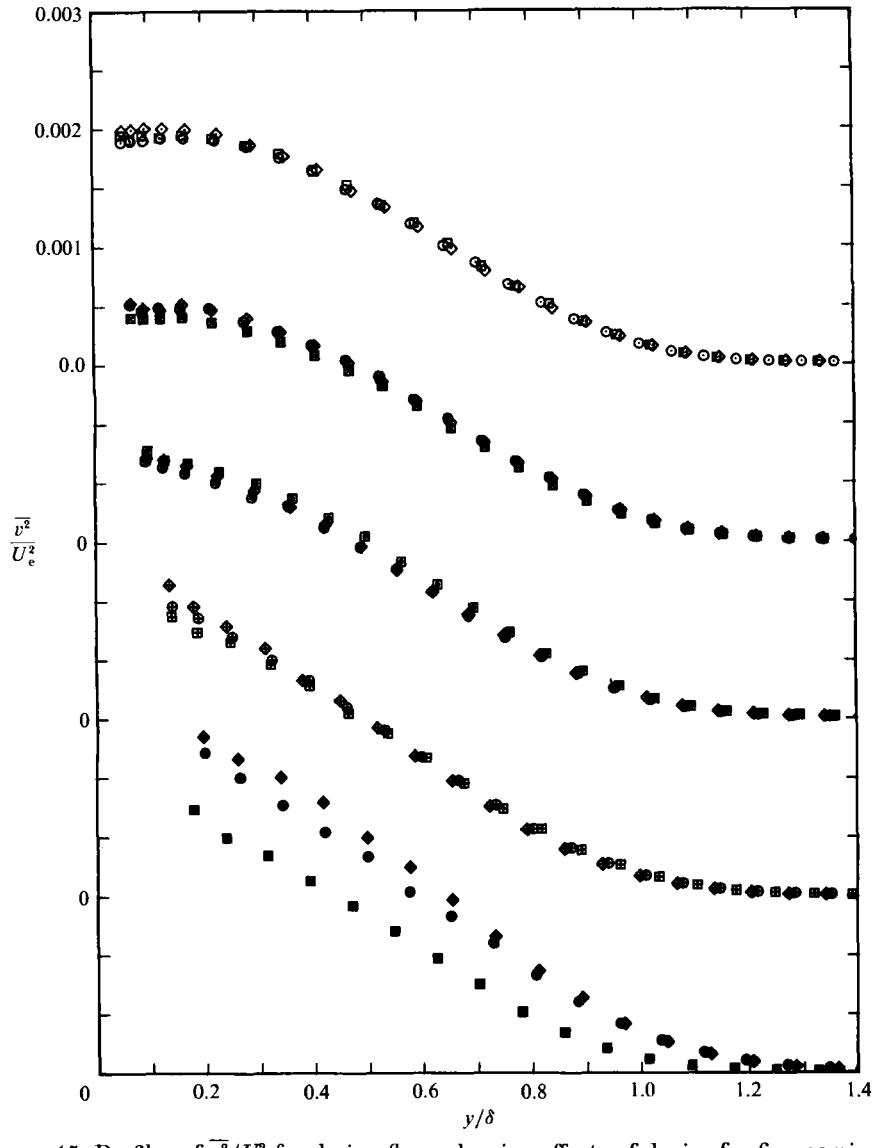

FIGURE 15. Profiles of $\overline{v^2}/U_e^2$ for design flows showing effects of device for five nominal values of R_θ. Note shift in ordinate. For explanation of symbols see figure 6.

The fact that the basic quantities of Reynolds stresses and triple products for the design flows for the different devices agree reasonably closely for $R_\theta \approx 1020$ and above means that parameters derived from these basic quantities will also not vary appreciably from device to device for $R_\theta \approx 1020$ and above. A wide range of derived turbulence quantities has been presented and discussed by Erm (1988). These consist of anisotropy parameters, skewness and flatness factors, terms in the balances of turbulent kinetic energy and Reynolds shear stress, eddy viscosities and mixing lengths, dissipation length parameters and turbulence transport velocities. Owing to space limitations, these are not given in this paper.

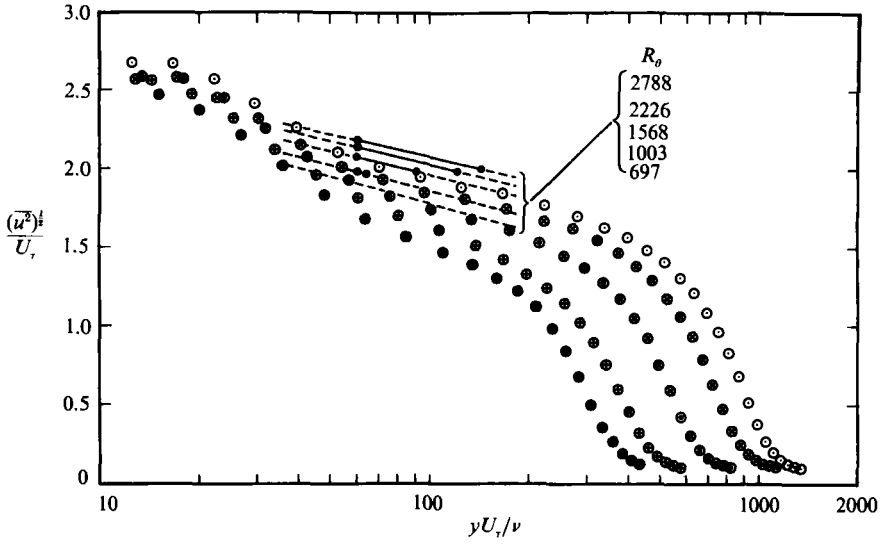

FIGURE 16. Profiles of $(\overline{u^2})^{\frac{1}{2}}/U_\tau$ for wire for design flow showing effects of R_θ. For explanation of symbols see figure 5. Predictions of Perry & Li (1990): ●——●, turbulent wall region; ----, outside turbulent wall region.

5.2. *Broadband-turbulence characteristics for under- and overstimulated flows*

Profiles of $\overline{u^2}/U_e^2$ used to determine the effects of under- and overstimulation for each of the devices are shown in figures 19 and 20 for $R_\theta \approx 1020$ and $R_\theta \approx 2175$ respectively. For $R_\theta \approx 1020$, the degree of stimulation noticeably affects profiles. The profiles for pins are affected significantly more than are the profiles for the wire and the grit, which are affected about equally. For $R_\theta \approx 2175$, the profiles for the wire and pins are now affected less, whereas the profiles for the grit are affected about the same. For $R_\theta \approx 1020$, and at $y/\delta = 0.4$, the maximum values in the overall range of variation of $\overline{u^2}/U_e^2$ for the wire, grit and pins are about 13%, 14% and 33% respectively greater than the corresponding minimum values. Corresponding numbers for $R_\theta \approx 2175$ are 7%, 13% and 9% respectively. It could be argued that some of the differences quoted are within experimental error, but the fact that trends for all devices correspond quite closely suggests that the observed differences are in fact real.

The fact that noticeable differences can occur within a given set of profiles may not have been fully appreciated by researchers in the past. Most likely researchers would have established a flow by comparing their measured ΔU^+ curve with that proposed by Coles (1962). However, an examination of such measured curves shown in figure 2 indicates that in a number of cases a curve for under- or overstimulated flow could quite easily be assumed to be acceptable if it was the only one measured in an investigation. This point should be borne in mind when assessing published turbulence data on low-Reynolds-number flows.

6. Analysis of spectra

6.1. *Spectral theory of Perry, Henbest & Chong*

Perry, Henbest & Chong (1986) have recently suggested a number of different ways of scaling spectra and they have also proposed spectral similarity laws. Their analysis

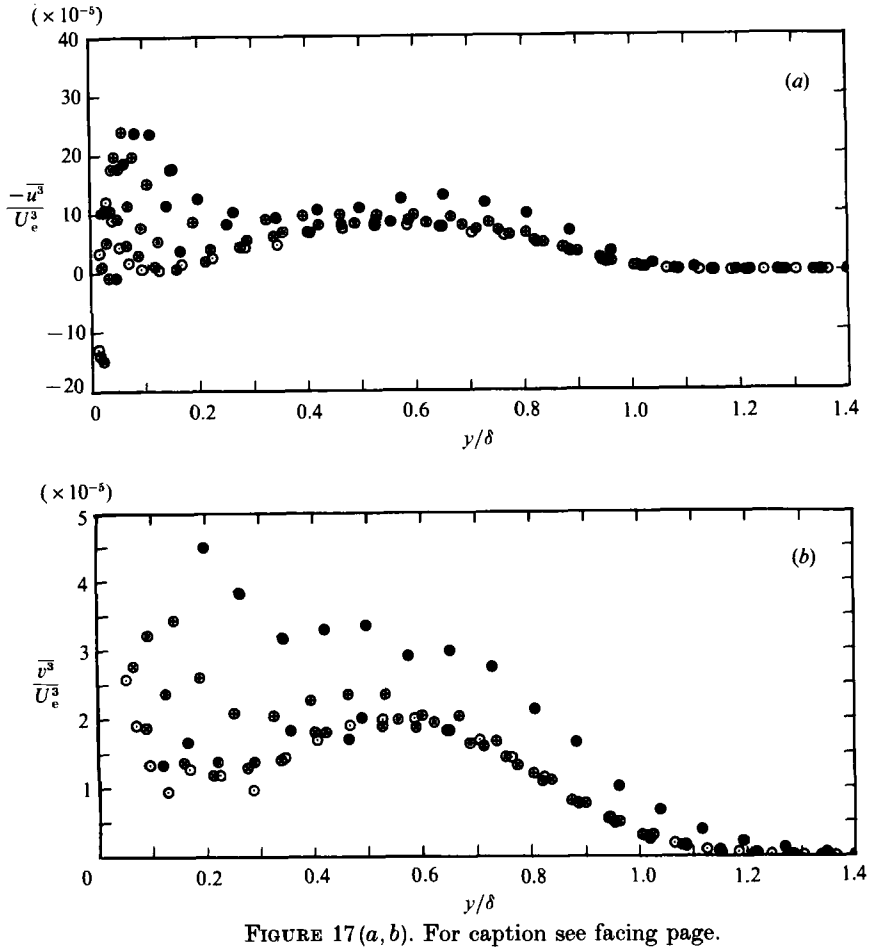

FIGURE 17 (*a*, *b*). For caption see facing page.

is only applicable to high-Reynolds-number, zero-pressure-gradient flows and was mainly applied to the turbulent wall region, which they defined as $\nu/U_\tau \ll y \ll \Delta_E$. The parameter Δ_E is an outer-flow lengthscale that scales with the boundary-layer thickness and has a value close to the 99% boundary-layer thickness. Although the theory was formulated for high-Reynolds-number flows, Spalart (1988) used their suggested scaling laws when plotting his numerically simulated low-Reynolds-number spectra. Since we also decided to make use of the theory, a brief description of some of its features is appropriate.

According to Perry *et al.* (1986), the behaviour of the u-spectra in the turbulent wall region can be separated into three wavenumber regions. Firstly, at low wavenumbers, the expected 'outer-flow' scaling law is of the form

$$\frac{\Phi_{11}[k_1\Delta_E]}{U_\tau^2} = f_1[k_1\Delta_E]. \tag{4}$$

$\Phi_{11}[k_1\Delta_E]$ is the power spectral density per unit non-dimensional wavenumber, $k_1\Delta_E$. Corresponding definitions apply to other power spectral densities having

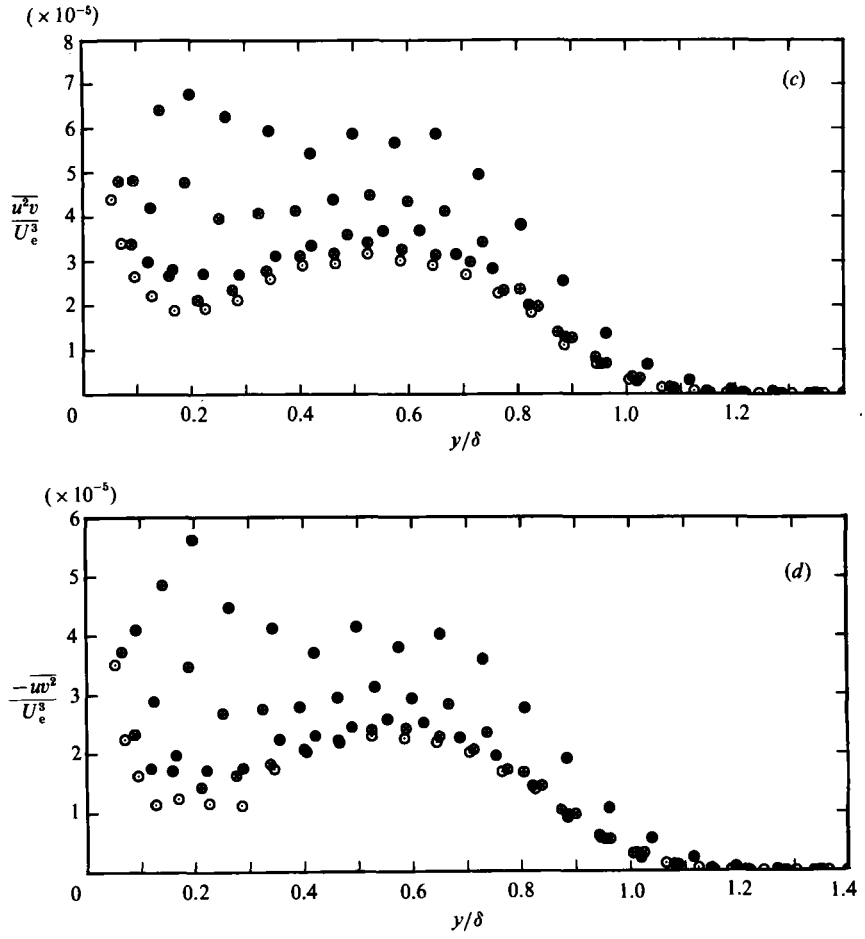

FIGURE 17. Profiles of triple products for wire for design flow showing effects of R_θ. (*a*) $-\overline{u^3}/U_e^3$; (*b*) $\overline{v^3}/U_e^3$; (*c*) $\overline{u^2v}/U_e^3$; (*d*) $-\overline{uv^2}/U_e^3$. For explanation of symbols see figure 5.

similar forms. Secondly, at moderate to high wavenumbers, the expected 'inner-flow' scaling law is of the form

$$\frac{\Phi_{11}[k_1 y]}{U_\tau^2} = f_2[k_1 y]. \tag{5}$$

Thirdly, at very high wavenumbers, the scaling of the u-spectra would be expected to follow the classical Kolmogorov (1941) viscosity-dependent scaling law,

$$\frac{\Phi_{11}[k_1 \eta]}{\upsilon^2} = f_3[k_1 \eta] \tag{6}$$

where η and υ are the Kolmogorov length and velocity scales respectively. For each of the above three types of scaling, spectra can generally be expected to collapse in the designated wavenumber region.

Equations (4) to (6) correspond to different u-spectral regions over the range of wavenumber k_1, and the theory anticipates two regions of overlap. The first of these is where (4) and (5) both apply simultaneously and in this region the spectra can be expected to collapse onto an inverse power-law distribution for both outer-flow and

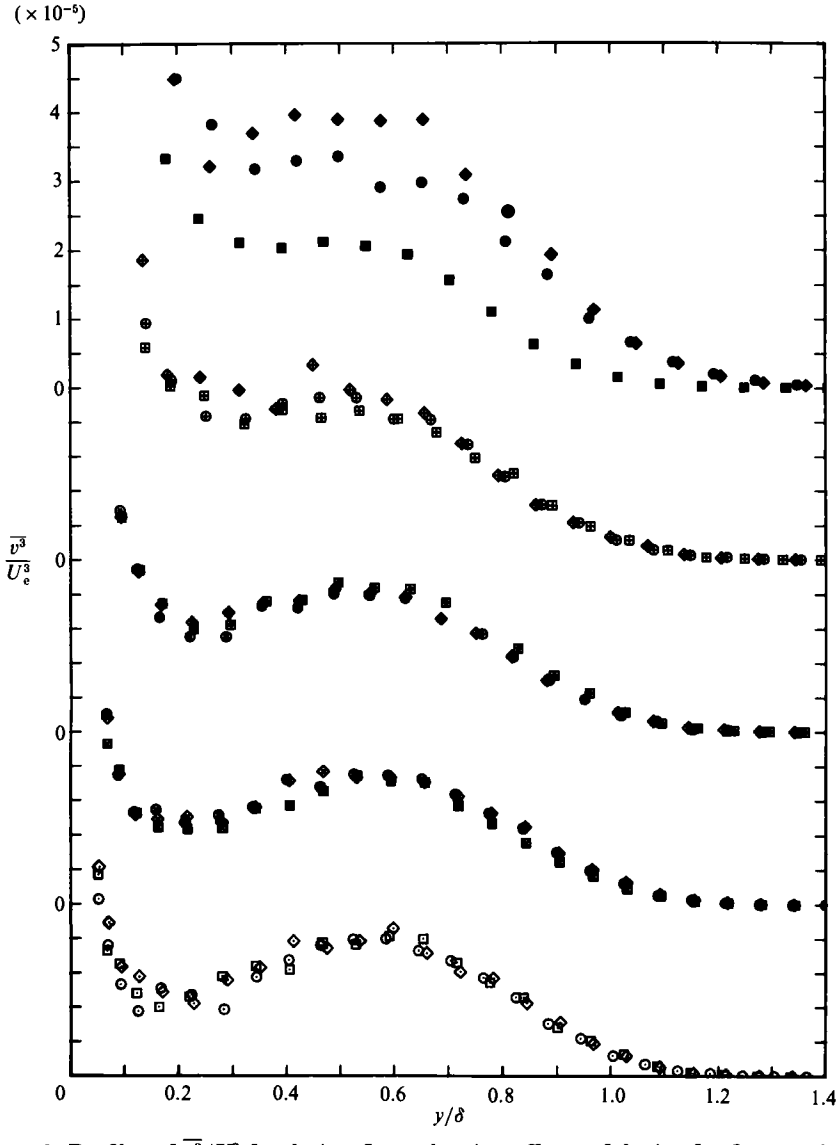

FIGURE 18. Profiles of $\overline{v^3}/U_e^3$ for design flows showing effects of device for five nominal values of R_θ. Note shift in ordinate. For explanation of symbols see figure 6.

inner-flow scaling. The second region of overlap is where (5) and (6) both apply simultaneously and in this region the spectra can be expected to collapse onto a $-\frac{5}{3}$ power-law distribution for both inner-flow and Kolmogorov scaling provided the Reynolds number of the flow is sufficiently large. This region of overlap is referred to as the inertial subrange.

The expected form of the w-spectra is similar to that for the u-spectra since u- and w-motions are similar. For the v-spectra, no outer-flow scaling law is expected and so there are only the inner-flow and Kolmogorov scaling laws and an overlapping region which is expected to follow a $-\frac{5}{3}$ power law.

Perry *et al.* (1986) also consider spectral behaviour in the fully turbulent region, which begins at the outer limit of the buffer zone and extends to the edge of the

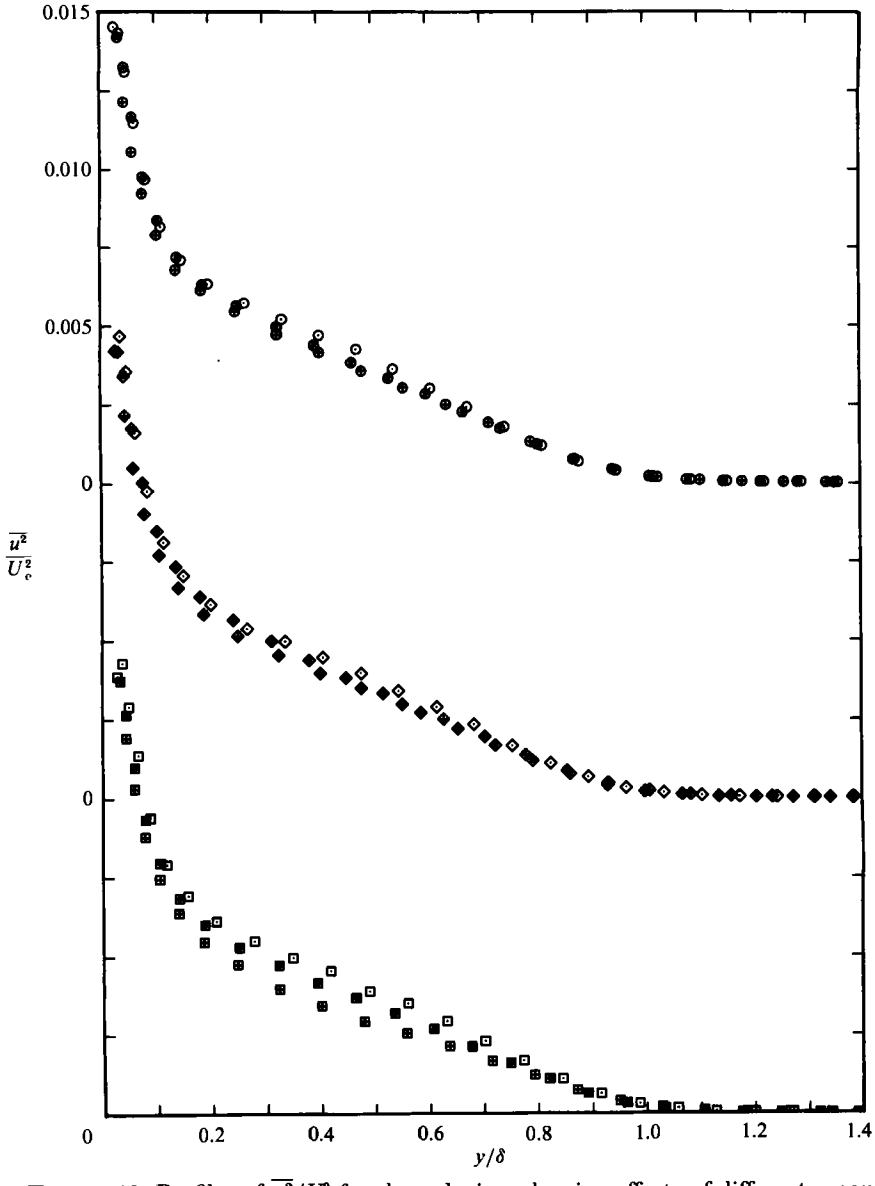

FIGURE 19. Profiles of $\overline{u^2}/U_e^2$ for three devices showing effects of different amounts of stimulation for $R_\theta \approx 1020$. Note shift in ordinate. For explanation of symbols see figure 11.

boundary layer. They indicate that the energy-containing region of the spectra of the u-component of the velocity fluctuations should follow

$$\frac{\Phi_{11}[k_1 y]}{U_\tau^2} = q_1\left[k_1 y, \frac{y}{\Delta_E}\right], \tag{7}$$

where q_1 is independent of viscosity. Similar expressions hold for the v- and w-components of the velocity fluctuations.

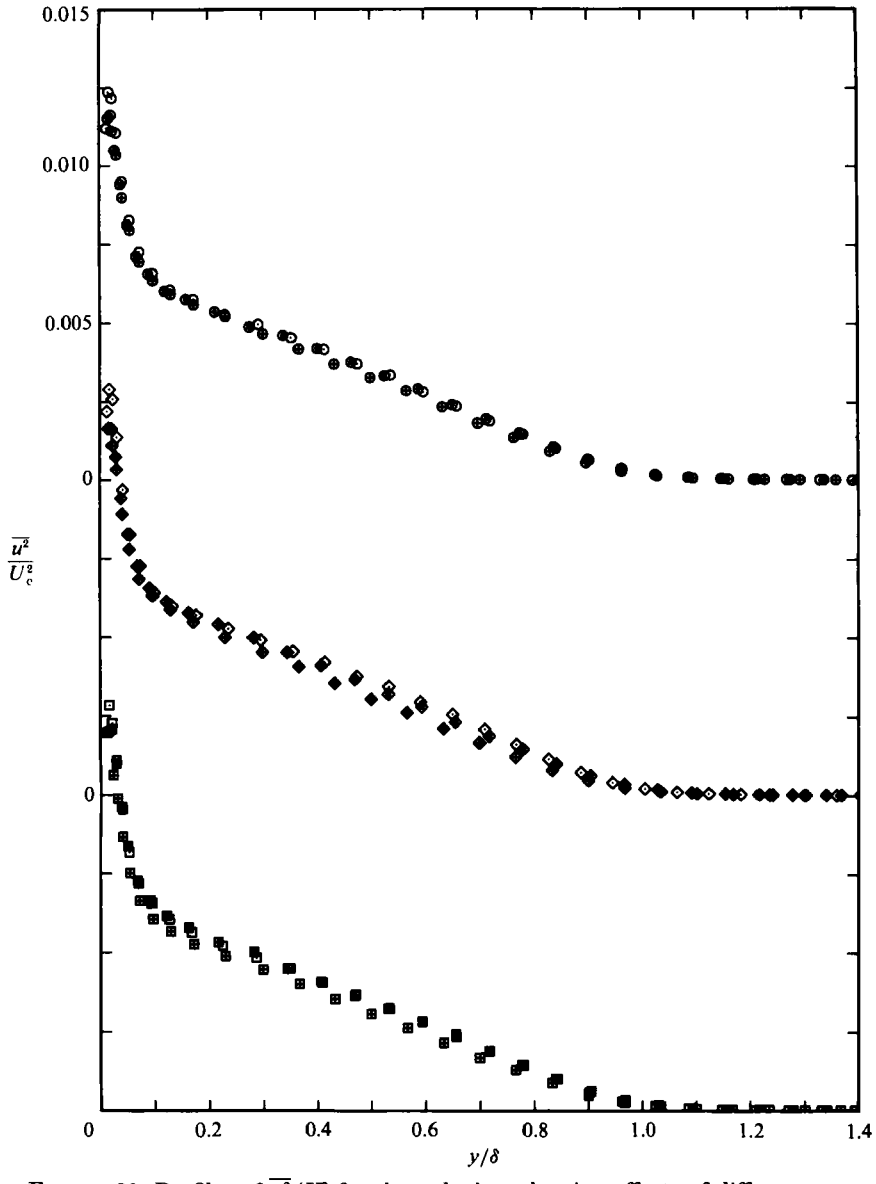

FIGURE 20. Profiles of $\overline{u^2}/U_e^2$ for three devices showing effects of different amounts of stimulation for $R_\theta \approx 2175$. Note shift in ordinate. For explanation of symbols see figure 12.

6.2. *Spectra for correctly stimulated flows*

The spectral plots to be presented will be abridged in a similar way to the plots for the broadband-turbulence characteristics.

6.2.1. *Spectra for the turbulent wall region*

It is of interest to see whether or not the current low-Reynolds-number spectra for the turbulent wall region follow the model of Perry *et al.* (1986). Perry *et al.* (1987) defined this region as $y^+ > 100$ and $y/\Delta_E < 0.15$ when applied to their smooth-wall boundary-layer flows. An analysis of current spectra indicated that for many of the

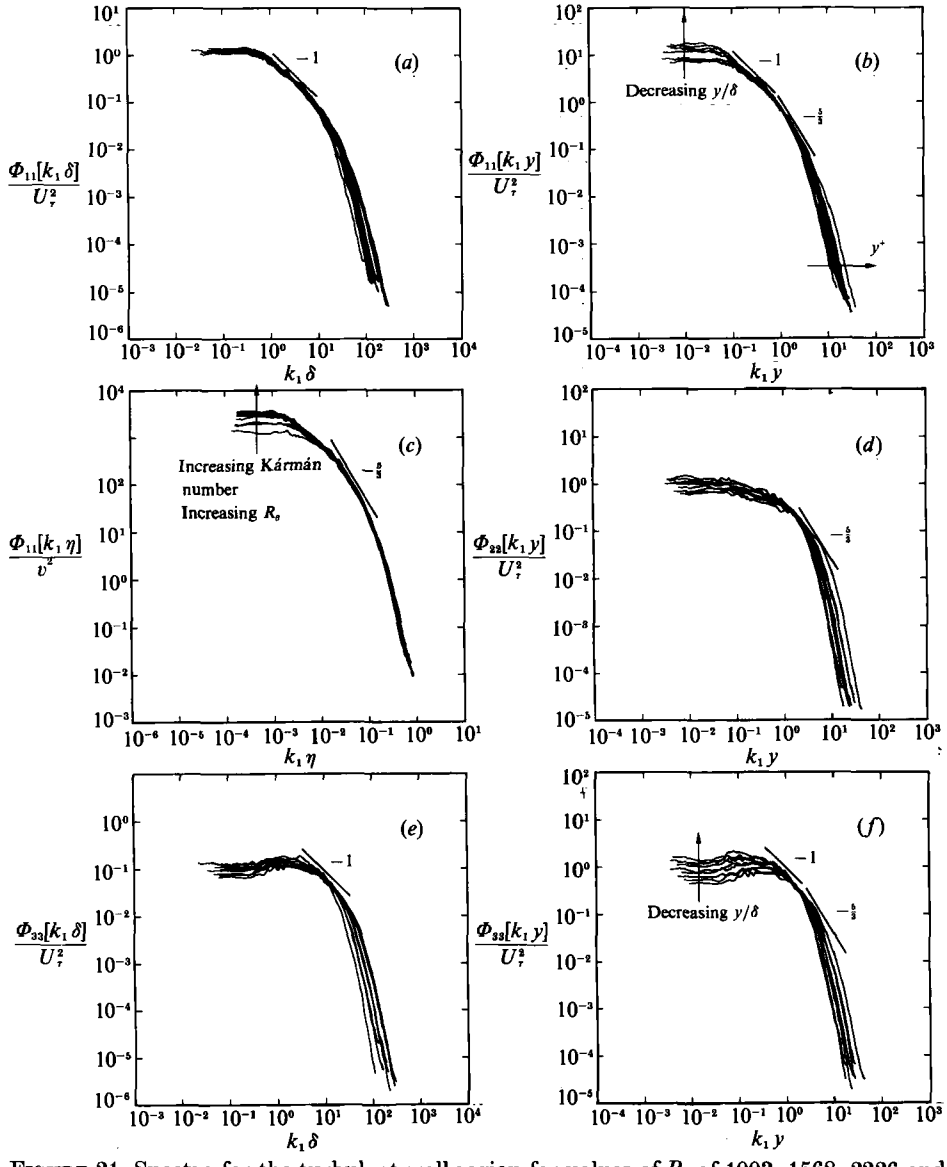

FIGURE 21. Spectra for the turbulent wall region for values of R_θ of 1003, 1568, 2226 and 2788 for wire for design flow. (*a*) *u*-spectra, outer-flow scaling; (*b*) *u*-spectra, inner-flow scaling; (*c*) *u*-spectra, Kolmogorov scaling; (*d*) *v*-spectra, inner-flow scaling; (*e*) *w*-spectra, outer-flow scaling; (*f*) *w*-spectra, inner-flow scaling.

families, the turbulent wall region defined using the above limits, but with Δ_E replaced by δ, the 99.5% boundary-layer thickness, just did not exist, i.e. when y^+ had attained a value of 100, then y/δ had already exceeded a value of 0.15. When Spalart (1988) used the theory of Perry *et al.* (1986), he adopted a less conservative definition for the turbulent wall region, namely $y^+ > 50$ and $y/\delta < 0.3$. For the current investigation it was also necessary to use a less restrictive definition and the limits chosen were $y^+ > 60$ and $y/\delta < 0.15$. The value of the first limit was chosen so that spectra corresponding to most of the values of R_θ were now accommodated in the definition of the turbulent wall region.

Spectra for the wire for the turbulent wall region are shown in figure 21 (*a–f*) for different types of scaling. The spectra correspond to values of R_θ of 1003, 1568, 2226 and 2788. No spectra for $R_\theta = 697$ are included, since for this value of R_θ the range chosen for the turbulent wall region did not exist. Lines of slope -1 and/or $-\frac{5}{3}$, corresponding to regions of collapse suggested by the model have been drawn on the plots.

The u-spectra plotted using outer-flow scaling, shown in figure 21 (*a*), collapse reasonably well onto an inverse-power-law region as anticipated by the model. Also, at low wavenumbers, the collapse of the spectra is quite good, which is also in accord with the model. According to Perry *et al.* (1986), any lack of collapse of the spectra at low wavenumbers can possibly be explained in terms of the invalid use of Taylor's (1938) hypothesis of frozen turbulence, which utilizes one single convection velocity for all eddy scales at a fixed point in the flow. The other question that must be addressed is whether the high wavenumber ends of the spectra peel off from the -1 line in order of decreasing values of y/δ for increasing values of $k_1\delta$, as anticipated by the model. A careful analysis of the spectra indicated that this was in fact the case for spectra corresponding to each of the values of R_θ, but for all spectra considered collectively, this behaviour was not followed.

For the u-spectra plotted using inner-flow scaling, shown in figure 21 (*b*), collapse onto an inverse-power-law region and a $-\frac{5}{3}$ inertial subrange is evident, as anticipated by the model. The low-wavenumber ends of the spectra peel off from the -1 line in order of decreasing y/δ for decreasing $k_1 y$, as predicted. A careful analysis of the spectra at their high-wavenumber ends indicated that, with minor exceptions, the spectra peeled off the $-\frac{5}{3}$ line in order of increasing y^+ for increasing $k_1 y$, as predicted.

The u-spectra plotted using Kolmogorov scaling, shown in figure 21 (*c*), collapse well at high wavenumbers as expected, and a short region of collapse onto a line of slope $-\frac{5}{3}$ can be discerned. The spectra at the low-wavenumber ends were found to peel off the $-\frac{5}{3}$ line in order of increasing Kármán number (see Perry, Lim & Henbest 1985), or alternatively increasing R_θ, for decreasing $k_1\eta$, and thus it is apparent that for higher values of R_θ, the extent of the region of collapse onto the line of slope $-\frac{5}{3}$ would most likely be greater, as was found by Perry *et al.* (1985) for their flows at higher values of R_θ.

For the v-spectra plotted using inner-flow scaling, shown in figure 21 (*d*), the theory anticipates collapse at the low-wavenumber ends and also collapse onto a line of slope $-\frac{5}{3}$ in the inertial subrange, and for the spectra shown this behaviour clearly does not apply. It appears that a -1 region exists for the v-spectra, which is contrary to predictions. Thus, their theory may not be applicable for v-spectra for low-Reynolds-number flows. In other ways, the v-spectra depart from the model in a similar manner to the spectra obtained by Perry *et al.* (1987). They state that the lack of collapse at low wavenumbers cannot be blamed on the spread in convection velocities as only eddies of scale of order y contribute significantly to $\overline{v^2}$ at y.

According to the model, the behaviour of the w-spectra plotted using outer-flow scaling, shown in figure 21 (*e*), should be similar to the behaviour of the corresponding u-spectra shown in figure 21 (*a*). For the w-spectra, collapse onto an inverse-power-law region is evident, but the extent of the collapse is shorter than for the corresponding u-spectra. The w-spectra clearly do not collapse at low wavenumbers, as they should according to the model, and this can possibly be explained by the invalid use of Taylor's hypothesis. The spread of the w-spectra at low wavenumbers is greater than the spread of the corresponding u-spectra, and this behaviour was also

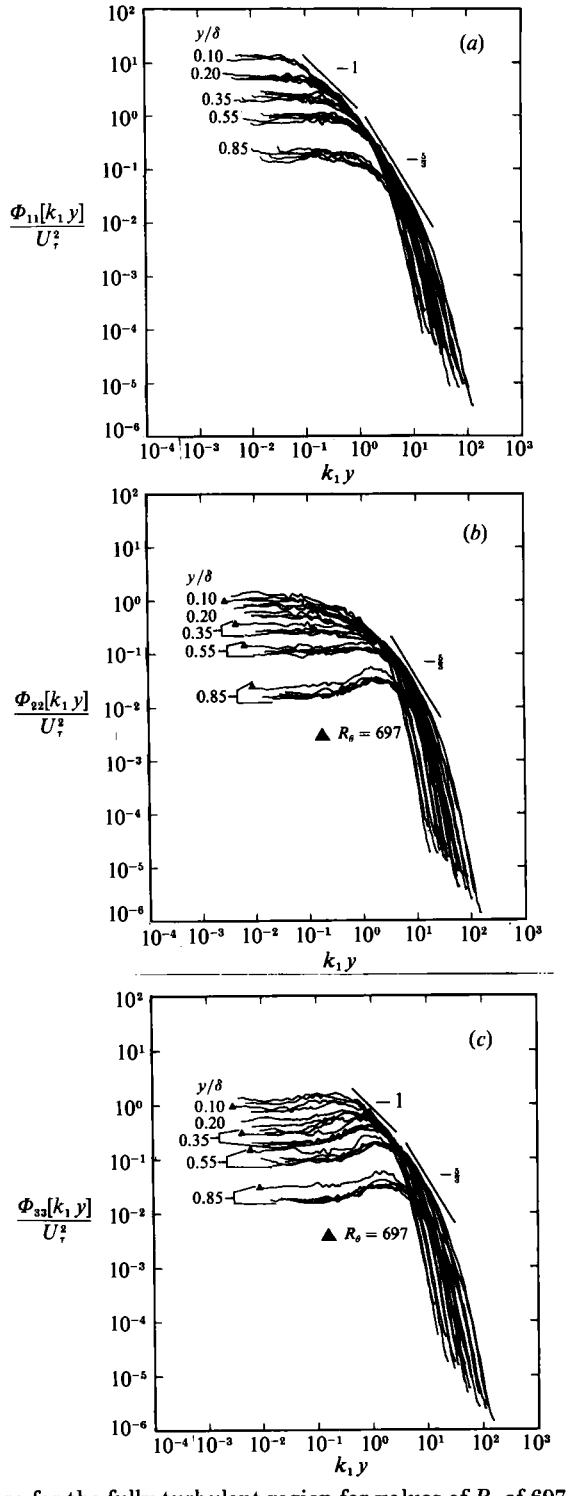

FIGURE 22. Spectra for the fully turbulent region for values of R_θ of 697, 1003, 1568, 2226 and 2788 for wire for design flow for various values of y/δ plotted using inner-flow scaling. (*a*) u-spectra; (*b*) v-spectra; (*c*) w-spectra.

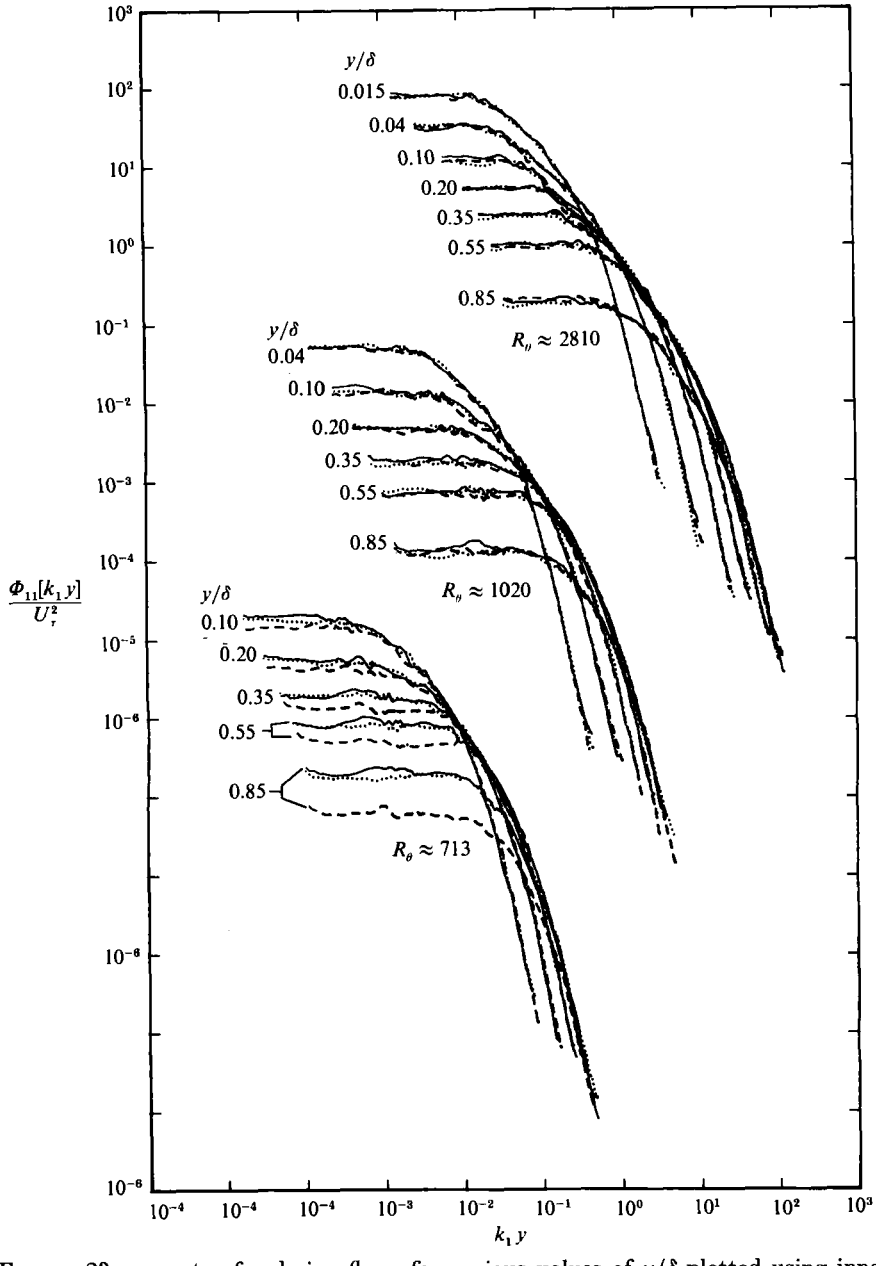

FIGURE 23. u-spectra for design flows for various values of y/δ plotted using inner-flow scaling showing effects of device for three nominal values of R_θ. Note shift in abscissa and ordinate: ——, wire; ....., grit; – – –, pins.

observed by Perry *et al.* (1987). The behaviour of the w-spectra at the high-wavenumber ends was similar to that for the corresponding u-spectra.

Finally, the behaviour of the w-spectra plotted using inner-flow scaling, shown in figure 21 (f), is expected to be similar to the u-spectra shown in figure 21 (b). On both figures, the spectra collapse onto an inverse-power-law region, but the extent of this region is less for the w-spectra than for the corresponding u-spectra, as was found by

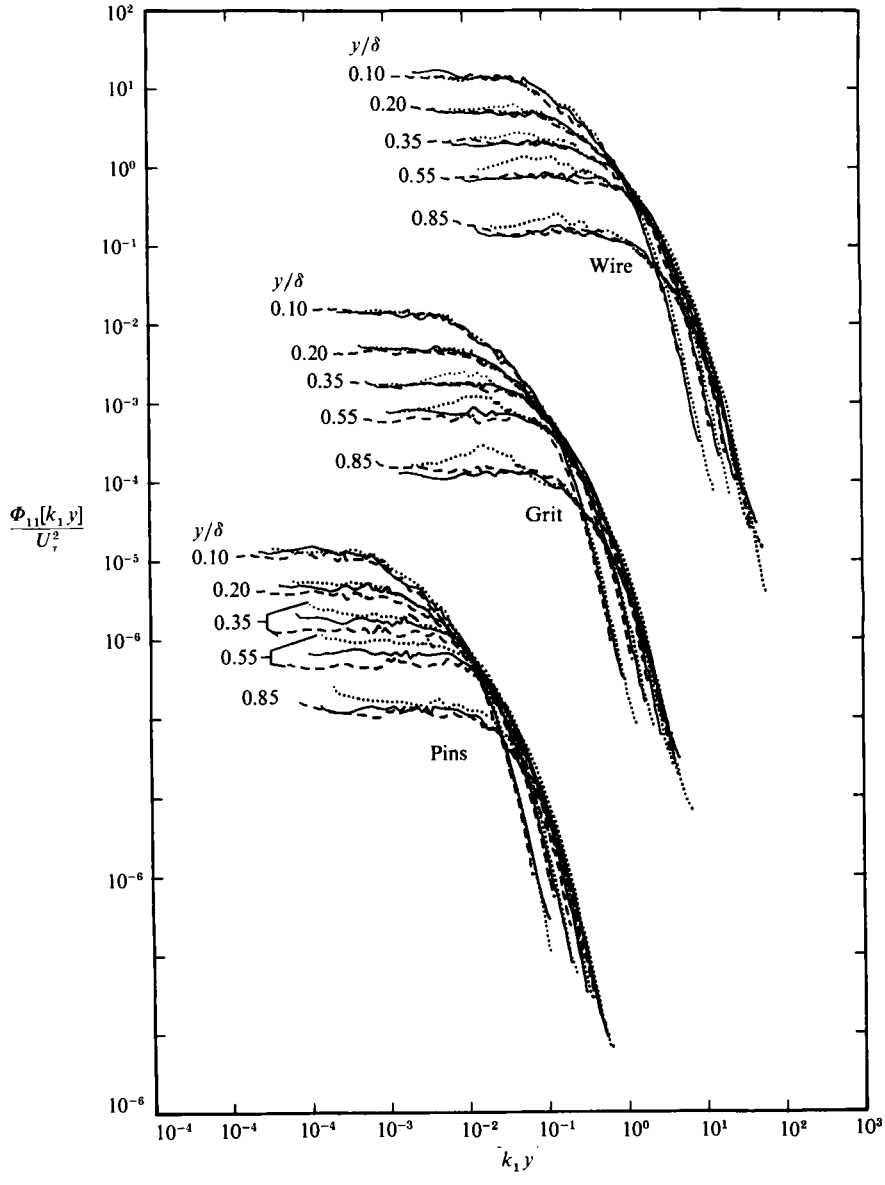

FIGURE 24. u-spectra for three devices showing effects of different amounts of stimulation at various values of y/δ plotted using inner-flow scaling. Note shift in abscissa and ordinate. Velocities given below are nominal values. Wire: ....., 8.0 m/s, $R_\theta = 1017$; ——, 10.0, 1003; – – –, 14.0, 1033. Grit: ....., 8.0 m/s, $R_\theta = 997$; ——, 10.0, 1042; – – –, 14.0, 1029. Pins: ....., 8.0 m/s, $R_\theta = 1024$; ——, 10.0, 1027; – – –, 14.0, 1013.

Perry *et al.* (1987). Collapse of the w-spectra in the inertial subrange is expected, but if collapse does occur, then it is only to a small extent, unlike for the u-spectra. With minor exceptions, the low-wavenumber ends of the spectra peeled off in order of decreasing y/δ for decreasing $k_1 y$, as predicted.

In Erm (1988), spectra are given for the turbulent wall region for the grit and pins corresponding to those shown in figure 21 (*a–f*) for the wire. The behaviour of the spectra for the grit and pins is shown to be similar to that for the wire.

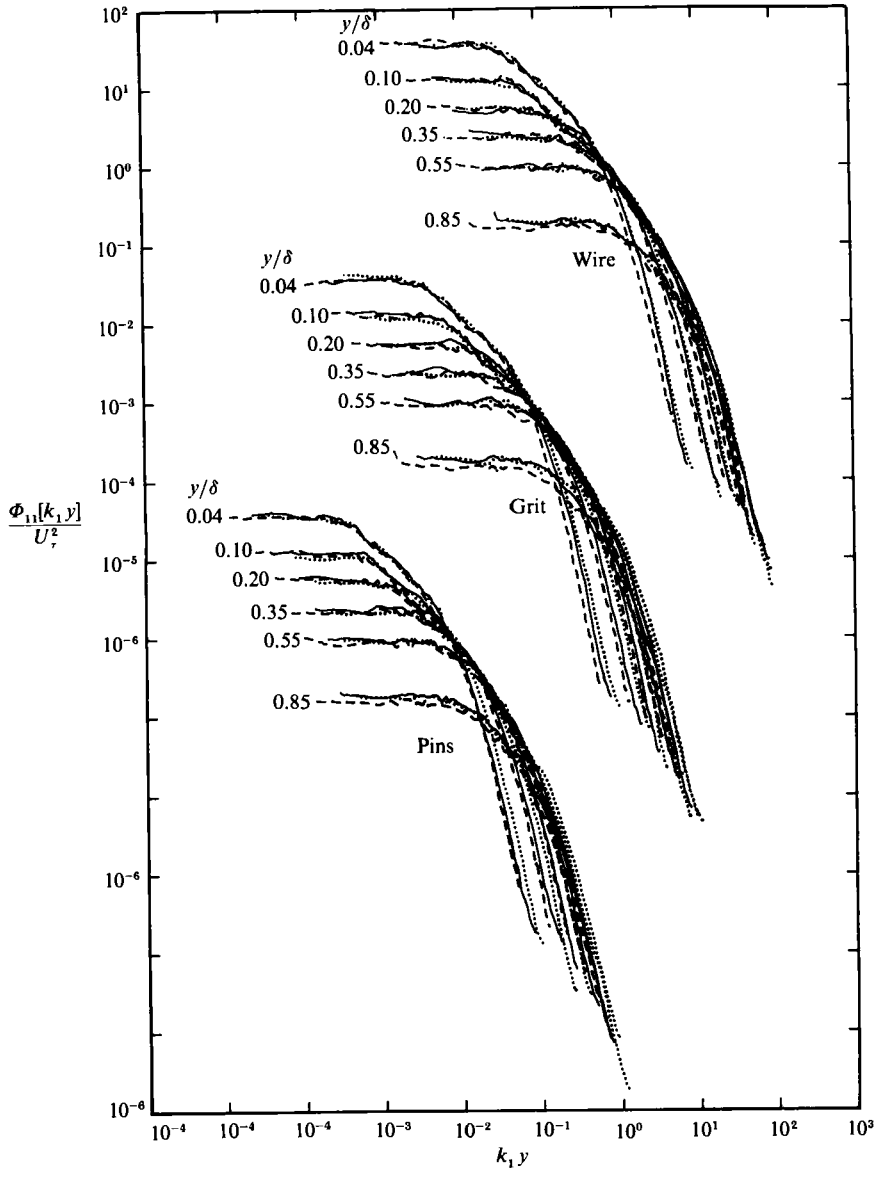

FIGURE 25. u-spectra for three devices showing effects of different amounts of stimulation at various values of y/δ plotted using inner-flow scaling. Note shift in abscissa and ordinate. Velocities given below are nominal values. Wire: ....., 8.0 m/s, $R_\theta = 2151$; ——, 10.0, 2226; – – –, 14.0, 2137. Grit: ....., 8.0 m/s, $R_\theta = 2146$; ——, 10.0, 2178; – – –, 14.0, 2119. Pins: ....., 8.0 m/s, $R_\theta = 2230$; ——, 10.0, 2181; – – –, 14.0, 2169.

It is encouraging that the low-Reynolds-number spectra, corresponding to values of R_θ as low as 1003, showed reasonably good agreement with the model, and where agreement did not occur, at least the spectra generally showed similar behaviour to those obtained by Perry *et al.* (1987) in their flat-plate boundary-layer study. This occurred despite the fact that the limits of the turbulent wall region had to be relaxed slightly to accommodate the spectra.

6.2.2. *Spectra for the fully turbulent region*

Equation (7) predicts that for the fully turbulent region, high-Reynolds-number spectra should collapse in the low-to-moderate wavenumber energy-containing range at each given value of y/δ and, if the Reynolds number of the flow is sufficiently large, the spectra for all values of y/δ should collapse onto an inertial subrange at high wavenumbers. It is thus of interest to see whether the current low-Reynolds-number spectra follow this law. Any deviations from the law will indicate the effects on spectral behaviour of variations in R_θ.

Some u-spectra for the wire, corresponding to five values of y/δ and five nominal values of R_θ, are plotted in figure 22 (a) using inner-flow scaling. Corresponding v- and w-spectra are shown in figures 22 (b) and 22 (c) respectively. At low wavenumbers, spectra within a given set generally show reasonable collapse, except sometimes for $R_\theta = 697$. Perry *et al.* (1986) also found slight spread at fixed values of y/Δ_E in their corresponding plot for u-spectra, and they indicated that this is thought to be due to a change in the fractional spread of the convection velocities of the eddies as the Reynolds number changes. This explanation could possibly also apply to the current spectra. The bands of the v- and w-spectra corresponding to $y/\delta = 0.1$ and 0.2 overlap and consequently have not been clearly indicated on figure 22 (b, c). The spectra obviously do not collapse at high wavenumbers and the closeness of the spectra at these wavenumbers makes it difficult to interpret spectral behaviour in this region. However, a careful analysis indicated that at high wavenumbers, the spectra at each value of y/δ peeled off in order of increasing R_θ as $k_1 y$ increased, a Reynolds-number effect also observed by Perry *et al.* (1986) for their u- and v-spectra.

6.2.3. *Effects of device on spectral behaviour*

As for the Reynolds stresses and triple products, it is only necessary to present spectra for one component of the turbulence to indicate effects of device on the u-, v- and w-spectra for different nominal values of R_θ. The u-spectra were chosen for the sample plots and these are shown in figure 23 for the three devices for different values of y/δ for nominal values of R_θ of 713, 1020 and 2810. The type of device used can have an appreciable effect upon spectra for $R_\theta \approx 713$, but for $R_\theta \approx 1020$ and above, the type of device used does not have a significant effect. For $R_\theta \approx 713$, the spectra for the wire and the grit agree quite well, but those for the pins differ from these.

6.3. *Spectra for under- and overstimulated flows*

Figures 24 and 25, for $R_\theta \approx 1020$ and $R_\theta \approx 2175$ respectively, show u-spectra used to determine the effects of under- and overstimulation for each of the devices. For $R_\theta \approx 1020$, the degree of stimulation has a marked effect on the spectra for all three devices and is most evident at the low-wavenumber ends. Differences are quite small at the lower values of y/δ, but tend to increase with increasing y/δ. For $R_\theta \approx 2175$, there is an overall general improvement in the agreement between corresponding spectra. Although some differences showing uniform trends often now occur at the high-wavenumber ends, the differences are only small.

7. Conclusions

The locations of the transition regions from laminar to turbulent flow for the wire, distributed grit and cylindrical pins tripping devices, as expressed in terms of C_f *vs.*

x curves, were found to vary with nominal reference velocity as it changed from 8.0 to 14.0 m/s. The stability of the transition region for the grit was found to be the most affected by changes in the velocity and that for the pins the least affected.

At the nominal design reference velocity of 10.0 m/s, the ΔU^+ *vs.* R_θ curves for each of the three devices agreed quite closely with the curve proposed by Coles (1962), but each often changed significantly for 8.0 and 14.0 m/s. The curve for the pins was the most sensitive to changes in velocity and that for the wire the least sensitive. The nine curves associated with the three devices and three velocities showed a general tendency to merge as R_θ increased so that the differences between them were minimal for $R_\theta \approx 3000$. The values of ΔU^+ for the nine flows decreased with reducing R_θ as expected, but they did not actually reach zero at the lower values of R_θ and in almost all cases the values of ΔU^+ at the lower values of R_θ increased with decreasing R_θ.

The lowest value of R_θ at which a logarithmic region was observed for a design-flow profile whose value of ΔU^+ was close to Coles' curve, was $R_\theta = 581$, and this profile was for the wire.

Transverse measurements of C_f for the three devices for the design flows were dissimilar in the early stages of development, but for $R_\theta \approx 2175$ and above, the data for the three devices agreed quite closely in corresponding cases and the type of device now had little influence on these measurements.

Mean-flow profiles for the design flows for each of the three devices, as well as corresponding Reynolds-stress and triple-product profiles for the wire, were shown to vary with R_θ for R_θ varying between about 715 and about 2810. The variation of the Reynolds stresses and triple products was found to be greatest in the wall region or slightly beyond when they were non-dimensionalized by U_e and plotted against y/δ. Although such measurements for low-Reynolds-number flows have been reported in the literature, there are no comprehensive measurements such as these near the wall.

Spectra were plotted using different types of scaling as given by Perry *et al.* (1986) and were compared with their models which were developed for high-Reynolds-number flows. For the turbulent wall region, it is encouraging that the low-Reynolds-number spectra for the design flow for the wire, corresponding to values of R_θ as low as 1003, showed reasonably good agreement with the model. Where agreement did not occur, at least the spectra generally showed similar behaviour to those of Perry *et al.* (1987) for their flat-plate boundary-layer study. For the fully turbulent region, it was found that although the current spectra for the design flow for the wire for R_θ varying between 697 and 2788 tended to obey predictions, some appreciable deviations were sometimes apparent, due to low-Reynolds-number effects.

For the design flows, mean-flow profiles, broadband-turbulence profiles and spectra were found to be affected very little by the type of device used for $R_\theta \approx 1020$ and above, indicating that the upstream history of the flow had little influence on these measurements within this R_θ range.

The degree of stimulation was found to have a noticeable effect on these types of measurements for $R_\theta \approx 1020$, but the differences were only convincing for the pins. There was a general overall improvement in agreement between measurements for $R_\theta \approx 2175$.

In previous studies, no researchers have investigated the effects of different devices or different amounts of stimulation on low-Reynolds-number flows, so the current data are especially significant in this respect.

The authors wish to thank Dr Seyed G. Saddoughi for his help throughout the investigation.

REFERENCES

BARLOW, R. S. & JOHNSTON, J. P. 1988 Structure of a turbulent boundary layer on a concave surface. *J. Fluid Mech.* **191**, 137.

BREDERODE, V. DE & BRADSHAW, P. 1974 A note on the empirical constants appearing in the logarithmic law for turbulent wall flows. *Imperial College Aero. Rep.* 74-03. Dept. Aeronautics, IC, London.

COLES, D. 1956 The law of the wake in the turbulent boundary layer. *J. Fluid Mech.* **1**, 191.

COLES, D. E. 1962 The turbulent boundary layer in a compressible fluid. Appendix A: A manual of experimental boundary-layer practice for low-speed flow. *Rand Rep.* R-403-PR.

COLES, D. E. 1968 The young persons guide to the data. In *Proc. Computation of Turbulent Boundary Layers, 1968, AFOSR-IFP-Stanford Conf.*, Vol. II (ed. D. E. Coles & E. A. Hirst).

ERM, L. P. 1988 Low-Reynolds-number turbulent boundary layers. Ph.D. thesis, University of Melbourne.

ERM, L. P., SMITS, A. J. & JOUBERT, P. N. 1987 Low Reynolds number turbulent boundary layers on a smooth flat surface in a zero pressure gradient. In *Turbulent Shear Flows 5* (ed. F. Durst, B. E. Launder, J. L. Lumley, F. W. Schmidt & J. H. Whitelaw). Springer. See also *Proc. Fifth Symp. on Turbulent Shear Flows, Cornell University, Ithaca, New York, Aug. 7–9, 1985.*

GRANVILLE, P. S. 1977 Drag and turbulent boundary layer of flat plates at low Reynolds numbers. *J. Ship Res.* **21**, 30.

HUFFMAN, G. D. & BRADSHAW, P. 1972 A note on von Kármán's constant in low Reynolds number turbulent flows. *J. Fluid Mech.* **53**, 45.

KOLMOGOROV, A. N. 1941 The local structure of turbulence in incompressible viscous fluid for very large Reynolds numbers. *CR Acad. Sci. URSS* **30**, 301.

KOVASZNAY, L. S. G. 1948 Spectrum of locally isotropic turbulence. *J. Aero. Sci.* **15**, 745.

LIGRANI, P. M. & BRADSHAW, P. 1987 Spatial resolution and measurement of turbulence in the viscous sublayer using subminiature hot-wire probes. *Exps. Fluids* **5**, 407.

MACMILLAN, F. A. 1956 Experiments on Pitot-tubes in shear flow. *Aero. Res. Counc. R. & M.* 3028.

MURLIS, J. 1975 The structure of a turbulent boundary layer at low Reynolds number. Ph.D. thesis, Imperial College, London.

MURLIS, J., TSAI, H. M. & BRADSHAW, P. 1982 The structure of turbulent boundary layers at low Reynolds numbers. *J. Fluid Mech.* **122**, 13.

PATEL, V. C. 1965 Calibration of the Preston tube and limitations on its use in pressure gradients. *J. Fluid Mech.* **23**, 185.

PERRY, A. E. 1982 *Hot-Wire Anemometry*. Oxford University Press.

PERRY, A. E., HENBEST, S. & CHONG, M. S. 1986 A theoretical and experimental study of wall turbulence. *J. Fluid Mech.* **165**, 163.

PERRY, A. E. & LI, J. D. 1990 Experimental support for the attached-eddy hypothesis in zero-pressure-gradient turbulent boundary layers. *J. Fluid Mech.* **218**, 405.

PERRY, A. E., LIM, K. L. & HENBEST, S. M. 1985 A spectral analysis of smooth flat-plate boundary layers. In *Proc. Fifth Symp. on Turbulent Shear Flows, Cornell University, Ithaca, New York, Aug. 7–9, 1985.*

PERRY, A. E., LIM, K. L. & HENBEST, S. M. 1987 An experimental study of the turbulence structure in smooth- and rough-wall boundary layers. *J. Fluid Mech.* **177**, 437.

PRESTON, J. H. 1958 The minimum Reynolds number for a turbulent boundary layer and the selection of a transition device. *J. Fluid Mech.* **3**, 373.

PURTELL, L. P. 1978 The turbulent boundary layer at low Reynolds number. Ph.D. thesis, University of Maryland.

PURTELL, L. P., KLEBANOFF, P. S. & BUCKLEY, F. T. 1981 Turbulent boundary layer at low Reynolds number. *Phys. Fluids* **24**, 802.

SIMPSON, R. L. 1970 Characteristics of turbulent boundary layers at low Reynolds numbers with and without transpiration. *J. Fluid Mech.* **42**, 769.

SMITS, A. J., MATHESON, N. & JOUBERT, P. N. 1983 Low-Reynolds-number turbulent boundary layers in zero and favourable pressure gradients. *J. Ship Res.* **27**, 147.

SPALART, P. R. 1988 Direct simulation of a turbulent boundary layer up to $R_\theta = 1410$. *J. Fluid Mech.* **187**, 61.

TAYLOR, G. I. 1938 The spectrum of turbulence. *Proc. R. Soc. Lond.* A **164**, 476.

WITT, H. T., WATMUFF, J. H. & JOUBERT, P. N. 1983 Some effects of rotation on turbulent boundary layers. In *Proc. Fourth Symp. on Turbulent Shear Flows, Karlsruhe, F. R. Germany, Sep. 12–14, 1983.*